

# Evolutionary properties of the low-luminosity galaxy population in the NGC 5044 Group<sup>\*</sup>

A. Buzzoni<sup>1</sup>, S. A. Cellone<sup>2,3</sup>, P. Saracco<sup>4</sup> & E. Zucca<sup>1</sup>

<sup>1</sup>*INAF - Osservatorio Astronomico di Bologna, Via Ranzani 1, 40127 Bologna, Italy*

*alberto.buzzoni@oabo.inaf.it, elena.zucca@oabo.inaf.it*

<sup>2</sup>*Facultad de Ciencias Astronómicas y Geofísicas, Universidad Nacional de La Plata, Paseo del Bosque, B1900FWA La Plata, Argentina*

<sup>3</sup>*IALP, CCT La Plata, CONICET-UNLP*

*scellone@fcaglp.unlp.edu.ar*

<sup>4</sup>*INAF - Osservatorio Astronomico di Brera, Via Brera 28, 20121 Milano, Italy*

*paolo.saracco@brera.inaf.it*

Received ; Accepted

## ABSTRACT

With this third paper of a series we present Johnson-Gunn  $B, g, V, r, i, z$  multicolour photometry for 79 objects, including a significant fraction of the faintest galaxies around NGC 5044, assessing group membership on the basis of apparent morphology (through accurate Sérsic profile fitting) and low-resolution ( $R = 500 - 1000$ ) optical spectroscopy to estimate redshift for 21 objects.

Early- and late-type systems are found to clearly separate in the Sérsic parameter space, with the well-known luminosity vs. shape relation being mostly traced by different morphological types spanning different ranges in the shape parameter  $n$ . A significantly blue colour is confirmed for Magellanic irregulars (Sm/Im's), while a drift toward bluer integrated colours is also an issue for dE's. Both features point to a moderate but pervasive star-formation activity even among nominally “quiescent” stellar systems. Together, dE's and Im's provide the bulk of the galaxy luminosity function, around  $M(g) \simeq -18.0 \pm 1.5$ , while the S0 and dSph components dominate, respectively, the bright and faint-end tails of the distribution. This special mix places the NGC 5044 group just “midway” between the high-density cosmic aggregation scale typical of galaxy clusters, and the low-density environment of looser galaxy clumps like our Local Group. The bright mass of the 136 member galaxies with available photometry and morphological classification, as inferred from appropriate M/L model fitting, amounts to a total of  $2.3 \cdot 10^{12} M_{\odot}$ . This is one seventh of the total dynamical mass of the group, according to its X-ray emission. Current SFR within the group turns to be about  $23 M_{\odot} \text{ yr}^{-1}$ , a figure that may however be slightly increased facing the evident activity among dwarf ellipticals, as shown by enhanced  $H\beta$  emission in their spectra.

Lick narrow-band indices have been computed for 17 galaxies, probing all the relevant atomic and molecular features in the 4300-5800 Å wavelength range. Dwarf ellipticals are found to share a sub-solar metallicity ( $-1.0 \lesssim [\text{Fe}/\text{H}] \lesssim -0.5$ ) with a clear decoupling between Iron and  $\alpha$  elements, as already established also for high-mass systems. Both dE's and dS0's are consistent with an old age, about one Hubble time, although a possible bias, toward higher values of age, may be induced by the gas emission affecting the  $H\beta$  strength.

**Key words:** galaxies: clusters: NGC 5044 group – galaxies: dwarf – galaxies: elliptical and lenticular, cD – galaxies: photometry – galaxies: fundamental parameters

<sup>\*</sup> Based on observations collected at the European Southern Observatory, La Silla (Chile) and at the CASLEO Observatory, op-

erated under agreement between CONICET, UNLP, UNC, and UNSJ, Argentina

## 1 INTRODUCTION

Low-mass and low-surface brightness (LSB) galaxies, including in this definition both dwarf ellipticals and irregulars, have since long surged to a central role in the general debate about galaxy formation and evolution. These objects, typically characterized by an absolute blue magnitude fainter than  $M_B \simeq -16$  and a mean surface brightness  $\langle \mu_e \rangle \gtrsim 22$  mag arcsec $^{-2}$  (Ferguson & Binggeli 1994), display in fact a quite wide range of morphological and spectrophotometric properties (e.g. Jerjen, Kalnajns & Binggeli 2000) such as to rise the question whether they assume an individual role as a sort of pristine building blocks to form more massive systems (as in the CDM theoretical scheme, e.g. Kaufmann et al. 1993), or they rather originate as coarse “by-products” of the formation of “standard” ellipticals and spirals (Knezek, Sembach, & Gallagher 1999; Lisker et al. 2007).

The problem of the genetic signature of low-mass systems is not a negligible one as, although in a more silent way, dwarf galaxies display in many cases continuous star formation activity, which makes them possible efficient “engines” to enrich the interstellar medium (e.g. Arimoto 1995). Actually, a major problem in this framework resides in the apparent dichotomy between active ongoing star formation, widely observed in LSB galaxies, and the exceedingly low metallicity of their present-day stellar populations (Arimoto & Tarrab 1990). The most striking case in this context is surely that of IZw 18, as recently discussed by Aloisi et al. (2007). Again, while for some dwarf ellipticals we might be dealing with a somewhat quiescent evolutionary scenario, reminiscent of old globular cluster history, in other situations a “tuned” star formation could have proceeded all over the entire galaxy life (e.g. Grebel 2005; Held 2005) still leaving, nowadays, an important fraction of fresh (primordial?) gas (e.g. Carrasco et al. 1995; Kuzio de Naray, McGaugh, & de Blok 2004).

As far as galaxy spatial distribution is concerned, the ubiquitous presence of LSB irregulars in the different cosmic environments (Cowie, Songaila, & Hu 1991; Ferguson & Binggeli 1994; Saracco et al. 1999) is clearly at odds with the morphology-density relation (Dressler 1980), which has been proven to hold for “standard” galaxies for a wide range of densities and scales (Postman & Geller 1984; Maia & da Costa 1990; Helsdon & Ponman 2003; Kelm, Focardi, & Sorrentino 2005). A systematic observational work to map the LSB galaxy distribution in selected zones of the sky has been carried out by different teams, leading to complete surveys and morphological catalogues of some loose groups of galaxies and nearby clusters (Binggeli, Sandage, & Tammann 1985; Karachentseva, Karachentsev, & Boerngen 1985; Ichikawa, Wakamatsu, & Okamura 1986; Davies et al. 1988; Ferguson 1989; Ferguson & Sandage 1990; Jerjen & Dressler 1997; Secker & Harris 1997).

These morphological surveys serve as a basic reference to any further spectrophotometric analysis of individual galaxies (Bothun & Mould 1988; Brodie & Huchra 1991; Cellone, Forte & Geisler 1994; Held & Mould 1994; Secker, Harris & Plummer 1997; Cellone 1999; Smith Castelli et al. 2008). However, efficient detection and accurate observation of LSB galaxies still remain

a formidable task, even for HST observations (e.g. Ferrarese et al. 2006) especially when moving to distances beyond the Virgo and Fornax Clusters, the two best studied aggregates so far (e.g. Hilker et al. 1999; Drinkwater et al. 2001; Conselice, Gallagher, & Wyse 2001; Deady et al. 2002; Mieske, Hilker, & Infante 2004; Gavazzi et al. 2005; Sabatini et al. 2005).

A complementary view may be gained through the study of smaller groups. In fact, the wide range of densities which characterizes these aggregates makes them the natural link between galaxy clusters and the field. Detailed mapping of the distribution and nature of low-mass galaxies in small groups will fill the “void” between fully relaxed systems (like actually the case of NGC 5044 group, e.g. Forbes 2007) to very loose and possibly unbound aggregates (Campos, Mendes de Oliveira, & Bolte 2004; Roberts et al. 2004). Besides probing the properties of dwarf galaxies in different environments, these have the advantage that even a moderate-sized sample would be fairly representative of the whole group population. At the same time, depth effects would be minimized allowing a better analysis of distance-dependent quantities.

In this work we want to further follow up a long-range study on the low-mass LSB galaxy population of the NGC 5044 group. In particular, after assessing group morphology and membership in previous contributions (Cellone & Buzzoni 2001, 2005), we would like to tackle here the problem of galaxy evolutionary properties, according to a multiwavelength observational approach that includes integrated and surface-brightness multicolour photometry, further complemented in most cases with a spectroscopic input. Our analysis will rely on original stellar population synthesis models, to which refer galaxy data in order to lead to a convenient and physically self-consistent picture of the galaxy evolutionary status for the NGC 5044 group.

In this framework, we will arrange our discussion by presenting the observed database in Sec. 2. Its morphological characterization will be carried out in Sec. 3 by fitting galaxy surface brightness with a Sérsic (1968) profile. These results in most cases refine our previous discussion in Cellone & Buzzoni (2005) leading also to a homogeneous morphological classification of the full galaxy population in the NGC 5044 group. Together with up-to-date redshift measurements, the revised morphological parameters proved to be a useful additional piece of information to constrain group membership and eventually assess the overall physical properties of the galaxy group as a whole. As a central step in this direction, in Sec. 4 we study galaxy distribution in different magnitude and colour domains. Starting from apparent magnitudes and morphological types, a match with the Buzzoni (2005) template galaxy models also allows us to lead to a realistic estimate of galaxy stellar mass and a reference birthrate figure for the galaxy group as a whole.

The spectroscopic properties for our sample are finally discussed in some detail in Sec. 5, where Lick narrow-band indices are derived for most of the observed galaxies. The diagnostic diagrams compare  $\alpha$ -element features, like Magnesium and Calcium, versus Iron and Balmer line strength, also including the contribution from Carbon molecules like CH (G band) and C $_2$ . We will discuss our results and summarize our main conclusions in Sec. 6.

## 2 OBSERVED DATABASE

Our galaxy sample consists of a total of 79 mostly dwarf and LSB galaxies, mainly selected from the Ferguson & Sandage (1990) catalogs, and representative of the faint galaxy population surrounding the standard elliptical NGC 5044, in the range  $-18 \lesssim M_B \lesssim -11$  mag,<sup>1</sup> regardless of morphology. Johnson *BV* photometry and *griz* imaging in the Gunn system (Thuan & Gunn 1976; Wade et al. 1979; Schneider, Gunn & Hoessel 1983), as well as mid-resolution ( $R = 500$ -1000) spectroscopy for a subsample of 24 objects have been collected during different observing runs from 1996 to 2000. Specifically, 40 objects have been observed during two observing campaigns (on the nights of Apr 16-17, 1999 and Apr 29-May 1, 2000) at the ESO 3.6m telescope of La Silla (Chile), while previous extended observations at the 2.15m telescope of the CASLEO observatory, in San Juan (Argentina) were carried out along three observing runs (on the nights of May 10-13 1996, Apr 8-10 1997, and Mar 19-21 1999) providing supplementary data for 57 galaxies, 18 of which in common with the ESO sample.<sup>2</sup>

### 2.1 Imaging

ESO observations have been carried out with EFOSC2, equipped with a Loral 2k CCD in a  $2 \times 2$  binned mode providing a platescale of 0.32 arcsec pixel<sup>-1</sup>. The  $5.3' \times 5.3'$  field of view allowed in most cases to image more than one galaxy within each frame. A total of 24 fields were imaged in the *griz* bands (see Fig. 1 in Cellone & Buzzoni 2005, for the exact location map), including 33 known low-luminosity galaxies, plus the bright Sbl-II NGC 5054, NGC 5044 itself, and 6 newly discovered LSB galaxies (see Cellone & Buzzoni 2005). Atmospheric conditions were photometric all the way, with sub-arcsec seeing during the first run, and a poorer performance (FWHM  $\gtrsim 1.5$  arcsec) in the 2000 run. In case of multiple exposures, a final image of the field was obtained by stacking the individual frames after all processing steps were completed. Standard stars from the lists of Schneider, Gunn & Hoessel (1983) and Jørgensen (1994) were also observed during each run for calibration purposes.

Johnson *BV* imaging at the CASLEO telescope has been carried out, on the other hand, during two runs in 1996 and 1999. The telescope was equipped with a Tektronix 1024x1024 CCD, providing a  $9'$  circular field of view in direct-imaging mode, with a platescale of 0.83 arcsec pixel<sup>-1</sup>. Standard stars for magnitude calibration were selected from the list of Landolt (1992). Seeing conditions were typically poorer than ESO observations, ranging between 2.0

and 2.8 arcsec. Partial results from the 1996 data have been presented in Cellone (1999).

Image processing of both ESO and CASLEO data was done using IRAF<sup>3</sup>, complemented with a few of our own FORTRAN routines. Each bias-corrected frame was twilight flat-fielded, while residual fringe patterns on ESO *i* and *z* images were corrected, mostly within a final  $\sim 1\%$  accuracy level, by subtraction of the appropriate templates (see Cellone & Buzzoni 2005, for more details on the procedure). Cosmic rays were cleaned up using the IRAF task COSMICRAYS, and the sky background, fitted with a tilted plane, was finally subtracted to obtain the final images of each field.

The photometric reduction procedure yielded a nominal figure ( $\sigma \sim 0.001$  mag) for the internal magnitude uncertainty of bright galaxies, being the total photometric error dominated throughout by the external uncertainty in the zero-point calibration. Overall, for a  $g \sim V \sim 16$  galaxy we estimate a full magnitude uncertainty of the order of  $\sigma \sim 0.03$  mag, a figure that may raise to  $\sigma \sim 0.06$  mag for the faintest ( $g \sim V \sim 21$ ) objects ( $\sigma \sim 0.10$  mag for CASLEO data).

A check of internal self-consistency of the *BV* photometry has been made possible by the combined observations of galaxies N49 ( $V = 16.5$ ) and N83A ( $V = 20.2$ ), in common to the 1996 and 1999 runs. For the first bright object, the coincidence was excellent, as both *B* and *V* isophotal magnitudes and surface brightness have been reproduced within  $\sim 0.004$  mag, and  $\sim 0.01$  mag arcsec<sup>-2</sup>, respectively. Much poorer is the match of N83A, instead, a very faint dSph galaxy. In the latter case, in fact, repeated *V* photometry resulted in a nearly negligible offset of 0.06 mag, that raised however to 0.35 mag for the *B* band. A similar figure has been found for the surface-brightness measurements, with a difference of 0.002 and 0.45 mag arcsec<sup>-2</sup> in *V* and *B*, respectively. This warns of the fact that photometric parameters of very faint galaxies may actually show considerable errors.

#### 2.1.1 Johnson to Gunn magnitude conversion

In order to ease a more homogenous discussion of the whole galaxy sample one would like to convert CASLEO *BV* photometry into ESO Gunn system. To this aim we took advantage of the 18 galaxies in common between the two subsamples, as summarized in Table 1. For these galaxies, integrated magnitudes within one *g*-effective radius, as identified by the Sérsic fitting profile (see Table A1), have been computed matching CASLEO *BV* and ESO *gr* photometry.

The linear fit to these data is reported in Table 2. One has to remark, however, that the strong clustering of the data in the colour domain (see Fig. 1), poorly constrains the relations of transformation. Alternatively, more standard sets of empirical conversion relationships can be found in the literature, mainly relying on the observation of stellar grids. This is the case, for instance, of the works by Jørgensen (1994) and Kent (1985), also reported in Table 2.

<sup>1</sup> For the NGC 5044 group a distance modulus ( $m-M$ ) = 31.96 – 5 log( $h_{100}$ ) can be estimated, according to the mean spectroscopic redshift of all group members in Cellone & Buzzoni (2005). For  $H_0 = 75$  km s<sup>-1</sup> Mpc<sup>-1</sup> this leads to a value of ( $m-M$ ) = 32.58 mag, that we will adopt throughout this paper.

<sup>2</sup> Here, and throughout the paper, the prefix “N” in our name coding of galaxies stands for the catalogue number in Ferguson & Sandage (1990). A supplementary letter “A”, “B”, or “C” to the standard catalog number refers to the newly discovered LSB galaxies of Cellone (1999); Cellone & Buzzoni (2005), and this paper, maintaining the reference number of the closest bright galaxy.

<sup>3</sup> IRAF is distributed by the National Optical Astronomy Observatories, which are operated by the Association of Universities for Research in Astronomy, Inc., under cooperative agreement with the National Science Foundation.

**Table 1.** Galaxy sample in common to CASLEO and ESO observing runs

Name	$\rho_e^S$ [arcsec]	Aperture magnitude			
		g	r	V	B
N30	10.90	15.939	15.526	15.835	16.712
N34	7.19	16.829	16.496	16.684	17.595
N42	17.49	15.723	15.435	15.508	16.342
N49	8.11	16.472	16.422	16.479	16.861
N50	7.16	15.938	15.524	15.811	16.588
N54	18.36	16.487	16.214	16.404	17.269
N54A	4.32	21.569	21.310	21.388	22.389
N55	5.26	20.151	19.757	20.021	20.636
N56	7.07	19.481	19.182	19.291	20.196
N62	7.76	19.840	19.470	19.261	20.429
N70	10.76	17.810	17.428	17.711	18.680
N70A	5.45	20.997	20.587	20.837	21.527
N75	7.74	16.009	15.652	15.915	16.825
N83	12.52	17.300	16.901	17.094	18.120
N83A	7.20	20.356	20.086	20.170	21.039
N109	7.30	18.301	18.066	18.207	18.916
N153	12.04	15.475	15.061	15.308	16.206
B3	2.41	18.346	17.755	18.226	19.741

**Table 2.**  $BV$  vs.  $gr$  conversion relationships

Least-square fit to the 18 galaxies in common			
$g-r = 0.33(B-V) + 0.05$	$(\sigma, \rho) = (0.08 \text{ mag}, 0.68)$		
$\pm 9$	$\pm 8$		
$B-g = 0.78(B-V) + 0.03$	$(\sigma, \rho) = (0.10 \text{ mag}, 0.86)$		
$\pm 11$	$\pm 10$		
Buzzoni (2005)			
$g-r = 0.78(B-V) - 0.25$	$(\Delta, \sigma) = (-0.10 \text{ mag}, 0.13 \text{ mag})$		
$B-g = 0.78(B-V) - 0.02$	$(\Delta, \sigma) = (0.05 \text{ mag}, 0.11 \text{ mag})$		
Jørgensen (1994)			
$g-r = 1.01(B-V) - 0.52$	$(\Delta, \sigma) = (-0.03 \text{ mag}, 0.18 \text{ mag})$		
$B-g = 0.50(B-V) + 0.23$	$(\Delta, \sigma) = (0.06 \text{ mag}, 0.13 \text{ mag})$		
Kent (1985)			
$g-r = 0.98(B-V) - 0.53$	$(\Delta, \sigma) = (0.00 \text{ mag}, 0.17 \text{ mag})$		
$B-g = 0.59(B-V) + 0.19$	$(\Delta, \sigma) = (0.01 \text{ mag}, 0.12 \text{ mag})$		

A further set of fully theoretical conversion equations has been considered in the table, relying on the Buzzoni (2005) template galaxy models. The latter calibration may in principle be more suitable for our aims, as it better accounts for the slightly different locus of stars and galaxies in the colour domain, given the “broader” spectral energy distribution (SED) of the latter.

The output of the different transformation sets is compared with our galaxy distribution in Fig. 1. None of the literature relations seems to suitably account for galaxy conversion along the entire colour range. On the other hand, one has also to consider that the bunching group of common objects in Table 1 is fairly representative of the bulk of CASLEO galaxies, as well (see the overplotted histogram in the lower panel of Fig. 1), and the few deviating targets at the most extreme colour edges are in fact among the faintest objects in the sample, possibly with highest internal uncertainty. To a closer analysis, and within the large scatter of the observations, one can notice a marginally more consistent match with the Buzzoni (2005) calibration, and we eventually decided to adopt this equation set for our CASLEO sample to be converted to Gunn magnitudes. According to Fig. 1, the (unweighted) external uncertainty provided by

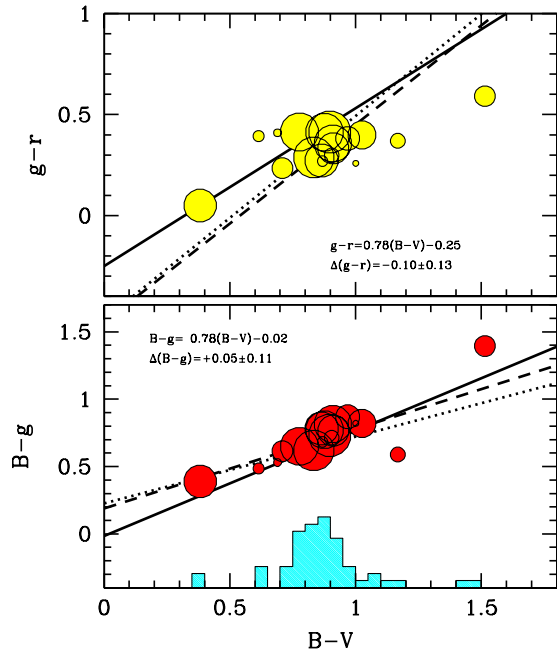


**Figure 1.** Gunn vs. Johnson system transformation for the 18 galaxies in common between ESO and CASLEO samples. For each object,  $g$ ,  $r$ ,  $V$ , and  $B$  aperture magnitudes (and the corresponding colours) refer to a fixed effective radius  $\rho_e^{[S]}$  as from the  $g$ -band Sérsic fitting profile, according to Table 1. Dotted and dashed lines are the relations of transformation by Kent (1985) and Jørgensen (1994), respectively, while solid line is the adopted Buzzoni (2005) calibration. The latter is explicitly reported in each panel, together with the mean uncertainty in converting  $(B - V)$  to  $(g - r)$  and  $(B - g)$  colours. Marker size in both panels is proportional to galaxy  $V$  luminosity. Note the bunched distribution of the calibrating galaxies, that closely traces the  $(B - V)$  distribution of the whole CASLEO sample, as sketched by the histogram in the lower panel.

the Buzzoni (2005) conversion equations (in the sense “observed” – “predicted”) amounts to  $\Delta(g - r) = -0.10 \pm 0.13$  and  $\Delta(B - g) = +0.05 \pm 0.11$  mag.

## 2.2 Spectroscopy

EFOSC2 has also been used in spectroscopic mode for ESO mid-resolution observations for a sub-sample of 24 galaxies (including NGC 5044 itself, the central galaxy of the group). Spectra along the 4300-6400 Å wavelength interval were obtained through a 1 arcsec longslit with ESO grism #8 and a 6 Å FWHM resolution ( $R \simeq 1000$ ) sampled at a scale of 2.1 Å pixel<sup>-1</sup>. When possible, a second target galaxy was included on the same spectrum frame of the main object. When no catalogued galaxy could be used as second target, we considered any likely background galaxy within the slit; six such objects were observed in this way (see Cellone & Buzzoni 2005, for details).

The ESO sample includes virtually all (three out of four) galaxies observed at CASLEO during the 1997 run in spectroscopic mode. The CASLEO observations were carried out with a Boller & Chivens spectrograph equipped with a 300 line mm<sup>-1</sup> dispersor grid, providing a FWHM resolution

of 9.5 Å ( $R \simeq 500$ ) along a bluer wavelength range (namely, from 3500–5700 Å) compared to ESO, sampled at bins of 4.4 Å pixel<sup>-1</sup>.

Each 2-D spectrum in our galaxy sample was bias-subtracted and flat-fielded via calibration spectra of an halogen lamp. One-dimensional spectra were extracted using IRAF standard routines, and wavelength-calibrated by means of He-Ne-Ar lamp technical exposures. Flux calibration of CASLEO and ESO (1999 run) spectra were carried out by means of the observation of spectrophotometric standard stars from the Baldwin & Stone (1984) catalog. Calibration of ESO 2000 observations relied instead on standard stars from the list of Gutiérrez-Moreno et al. (1988).

Finally, individual 1-D spectra were coadded to obtain the fiducial spectrum of each target. Cross-correlation with the spectrum of NGC 5044, used as a template, provided eventually a measure of the redshift of each object in the ESO sample, as we already discussed in Cellone & Buzzoni (2005). A redshift of  $cz = 2351 \pm 71 \text{ km s}^{-1}$  was derived, independently, for galaxy N29, the only one observed at CASLEO with no ESO counterpart.

### 3 MORPHOLOGICAL PARAMETERS

An accurate morphological study for 33 galaxies in our sample has already been undertaken in Cellone & Buzzoni (2005), providing a (re)classification and membership estimate of most objects on the basis of their image properties and, wherever possible, of the available spectroscopic redshift. Taking previous analysis as a reference, we want here to complete our review for the whole galaxy set.

We took advantage for our classification of the “objective” shape parameters, as provided by a Sérsic (1968) fit of radial surface brightness profile ( $\mu(\rho)$ ), i.e.

$$\mu = \mu_0 + 1.086 \left( \frac{\rho}{\rho_0} \right)^n. \quad (1)$$

In this scheme, three parameters constrain galaxy morphology, namely a central surface brightness ( $\mu_0$ ), a scale radius ( $\rho_0$ ), and a “shape index”  $n$  (being, as a reference,  $n = 0.25$  for the standard de Vaucouleurs profile), which discriminates between “spiky” ( $n < 1$ ) and “cored” ( $n > 1$ ) galaxies. While many bright dE/dS0 do show composite structure (i.e. “bulge”+“disk”, see Cellone 1999; Cellone & Buzzoni 2001), we did not attempt here to make any profile decomposition; Sérsic shape parameter  $n$  thus traces the global morphology of each galaxy. All the calculations made use of the  $g$ -band or the  $V$ -band observations for the ESO and CASLEO subsamples, respectively.

Given the different PSFs between the ESO and CASLEO observations, instead of trying to correct for seeing effects, we chose a simpler—and safer—approach, following Cellone (1999), who showed that seeing induced errors on the fitted Sérsic parameters tend to be negligible when an inner cutoff radius  $\approx 2 \times \text{FWHM}$  is used for the fits (see also Gavazzi et al. 2005). An outer cutoff at a radius where  $S/N \simeq 1$  prevents against systematic errors due to an imperfect sky subtraction. While the choice for the inner cutoff turned out to have no impact on the ESO data, thanks to their superior seeing, some limitation might be expected, in

principle, for the fit of CASLEO galaxies, one third of which being comprised with their scale radius within  $2 \times \text{FWHM}$ .

A summary of the results for the whole galaxy sample is displayed in Tables A1 and A2.<sup>4</sup>

In addition to the fitting morphological parameters ( $\mu_0$ ,  $\rho_0$  and  $n$  appear, respectively in col. 8, 9, and 10 of the tables), we also provided a more direct estimate of galaxy size, assumed to coincide with the isophotal radius ( $\rho_{27}$ ) at  $\mu(g) = 27 \text{ mag arcsec}^{-2}$ , and of effective radius ( $\rho_e$ ), which encircles 50% of the luminosity within  $\rho_{27}$  (see cols. 6 and 7 in the tables, respectively).<sup>5</sup>

The 18 galaxies in common between the ESO and CASLEO subsamples provided a useful cross-check, allowing us to consistently compare the  $V$  vs.  $g$  fits. For the measured values of  $\rho_e$ , this is shown in the upper panel of Fig. 2, where one can appreciate a nice relationship in place between the two sets of observations with just one evident outlier, that is galaxy N62 among the faintest and most vanishing objects in the sample (see Fig. 2 in Cellone & Buzzoni 2005). After rejecting this object, we have that CASLEO effective radii match the corresponding ESO figures within a  $\pm 11\%$  relative uncertainty. An external check of the accuracy in the fitting procedure can be obtained from the analysis of the lower panel of Fig. 2, where the “observed” value of  $\rho_e$  is matched with the corresponding parameter inferred from the Sérsic fit ( $\rho_e^{[S]}$ ).<sup>6</sup> The two estimates agree within a  $\pm 9\%$  relative scatter, after a  $3\text{-}\sigma$  rejection of three relevant outliers, namely the two dSph galaxies N94A and B (from the CASLEO sample) and the (background?) elliptical N139 (from the ESO sample), as singled out in the figure. Regarding the shape parameter  $n$ , which is particularly sensible to differing seeing conditions and sky-subtraction errors, we also obtain a good agreement ( $\langle \Delta n \rangle = -0.07 \pm 0.04$ ) between ESO-CASLEO samples when the 12 brighter ( $g_{27} < 18$ ) galaxies are considered, while a poorer match ( $\langle \Delta n \rangle = 0.23 \pm 0.12$ ) is attained for the 6 fainter systems.

It is of special interest to explore the  $n$ -index distribution across the Hubble/de Vaucouleurs morphological type of our galaxies. The latter has been inferred from a careful “eye-driven” standard classification of the original images, complementing the previous Cellone & Buzzoni (2005) results (see the “CB05” column in Tables A1 and A2). Given a better observing material, our types refine and update, in most cases, the original scheme by Ferguson & Sandage (1990) (column “FS90” in the tables). At the same time, our revised morphological classification led membership re-assessment for galaxies with no redshift available (see

<sup>4</sup> Note that among the CASLEO galaxies, a more careful inspection of the observed fields also led us to discover 6 more LSB galaxies (all consistent with a dSph morphology), not reported ever. For reader’s better convenience, their coordinates are summarized in Table A3 of the Appendix.

<sup>5</sup> The approximation of  $\rho_{\text{gal}}$  with  $\rho_{27}$  might lead of course to a slightly underestimated galaxy total luminosity, an effect mostly contained within  $\sim 0.2 \text{ mag}$ , as shown by Cellone & Buzzoni (2005, see Fig. 5 therein).

<sup>6</sup> Given a Sérsic scale length parameter,  $\rho_0$ , the fitting effective radius  $\rho_e$  can be defined as  $\rho_e/\rho_0 = w^n$ , where the parameter  $w = w(n)$  comes from the (numerical) solution of the relevant relation  $\Gamma(2/n)/2 = \gamma(2/n, w)$ , with  $\Gamma$  and  $\gamma$  being respectively the complete and incomplete Gamma functions.

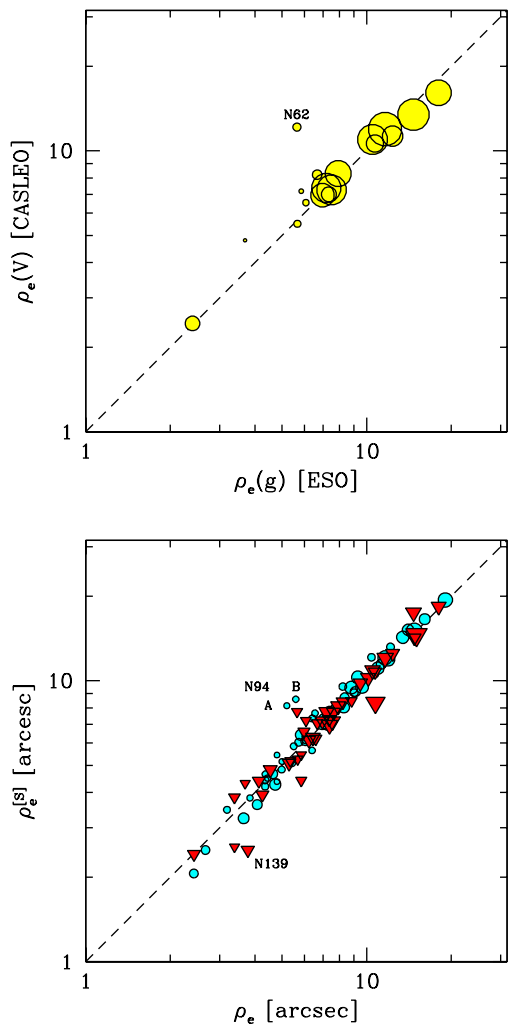


**Figure 2.** *Upper panel:* A combined comparison of the observed effective radius  $\rho_e$  (in arcsec) in the  $V$  and  $g$  bands for the 18 galaxies in common between ESO and CASLEO samples. The two measures are consistent within a  $\pm 11\%$  relative uncertainty. *Lower panel:* Observed ( $\rho_e$ ) vs. computed ( $\rho_e^{[S]}$ ) values of the effective radius, the latter as from the Sérsic fitting profile, for the whole (ESO+CASLEO) sample of 79 galaxies. The two estimates agree within a  $\pm 9\%$  relative scatter. Marker size is proportional to galaxy  $g$  or  $V$  luminosity, respectively, with CASLEO objects plotted as dots, and ESO objects as triangles. See the text for a brief discussion of the few outliers in both panels.

Cellone & Buzzoni 2007). A new set of radial velocity measurements, recently provided by Mendel et al. (2008), raised to 45 the number of galaxies with available redshift in our sample. In most cases, the morphologically assigned membership status (see the corresponding code,  $m_c$ , in col. 2 of Tables A1 and A2) was confirmed by the new redshifts, while just for three galaxies it had to be changed (from  $m_c = 3$  to  $m_c = 1$ ), leading also to changes in their respective morphological types (as from col. 5 of Tables A1 and A2).

The match of the refined morphological types with the Sérsic shape index is summarized in Fig. 3. As expected, the  $n$ -index properly accounts for the disk vs. bulge relative contribution to galaxy luminosity. In particular, bulge-

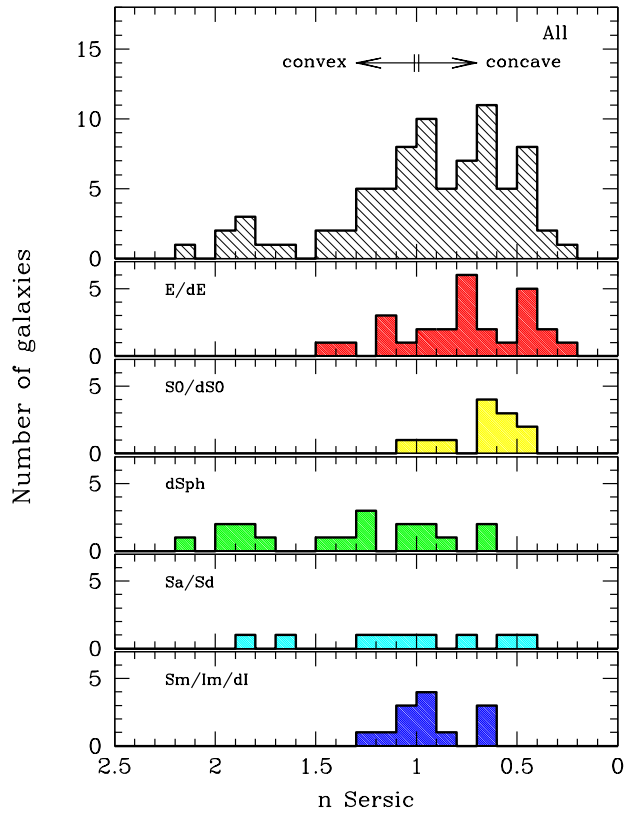


**Figure 3.** Galaxy distribution according to the Sérsic shape fitting parameter “ $n$ ” of eq. (1), as reported in Table A1 and A2. For the galaxies with both CASLEO and ESO observations the latter data have been used. Compared to a perfect exponential case ( $n = 1$ ), a “convex” surface-brightness radial profile has to be expected for  $n > 1$ , while a “concave” one is generated for  $n < 1$ , as labelled in the top panel, that collects the whole sample of 79 objects. The lower panels disaggregate the galaxy population according to the morphological classification. See text for a discussion.

dominated systems (E/dE+S0/dS0) are shown to display, on average, a “concave” ( $n < 1$ ) surface-brightness profile, while disk-dominated systems (Sa/Sd) span the full range of the  $n$  index according to a wider disk/bulge luminosity partition. A shallower brightness profile also characterizes dwarf spheroidal (dSph) systems, where a cored structure likely leads to a “convex” ( $n > 1$ ) shape index. A pure exponential profile ( $n \simeq 1$ ) is, on the contrary, the distinctive feature of later-type galaxies (Im/dI), that lack any clear nuclear condensation. To much extent, such a morphological segregation for the Sérsic shape index is the ultimate responsible for the observed trend of  $n$  with galaxy luminosity (e.g. Cellone 1999). As we will see in the next section, in fact, early-type (low- $n$ ) systems are among the brightest group members, while dSph (high- $n$ ) galaxies preferentially populate the faint-end tail of the group luminosity function. On a similar argument, the same effect neatly stems, as well, from a study of the  $\mu_0$  vs.  $n$  Sérsic parameters, like in Fig. 4.

The plot shows, in addition, that early-type profiles actually tend to smoothly match the standard de Vaucouleurs case ( $n \rightarrow 0.25$ ) as far as galaxy luminosity (and accordingly  $\mu_0$ ) brightens up reaching the distinctive range of “standard”

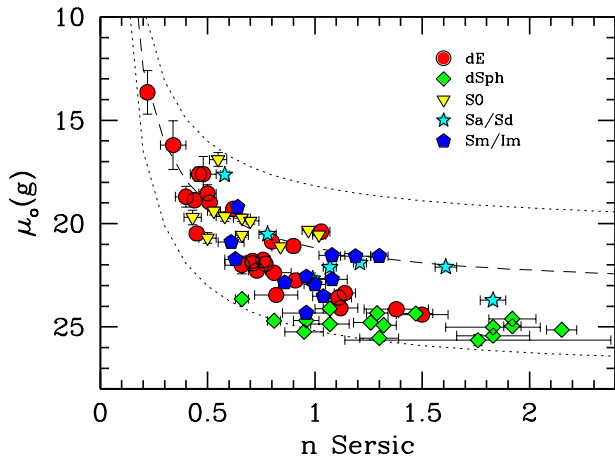


**Figure 4.** The central surface brightness ( $\mu_0(g)$ ) is compared with the shape parameter  $n$ , both as from the  $g$ - or  $V$ -band Sérsic fitting profile for the whole galaxy sample (see Table A1 and A2). In lack of ESO observations, CASLEO  $V$  data have been used, after converting to  $g$  magnitudes according to the adopted calibration of Table 2. The three overplotted curves mark the locus for fixed mean effective surface brightness, namely  $\langle \mu_{g_e} \rangle = 23 \text{ mag arcsec}^{-2}$  (middle dashed curve), and  $\langle \mu_{g_e} \rangle = 20$  and  $27 \text{ mag arcsec}^{-2}$  (upper and lower dotted curves, respectively). Galaxy marker depends on morphological type, as labelled on the plot. Note a clear morphological segregation of the different groups, with a prevailing presence of dSph’s among the LSB galaxy component, while ellipticals are among the brightest members approaching the standard de Vaucouleurs profile for  $n \rightarrow 0.25$ .

ellipticals, as confirmed by the straight  $L - n$  observed relationship. At the faint end, dSph’s display a wide range in  $n$ , while their central surface brightnesses remain almost constant at  $\mu_0(g) \approx 25 \text{ mag arcsec}^{-2}$ .

#### 4 PHOTOMETRIC PROPERTIES

The Gunn  $griz$  magnitudes and the Johnson  $BV$  photometry provide a minimal but effective set of measures to probe galaxy SEDs along the 4400-9000 Å wavelength range. In addition to the morphological piece of information, in fact, a multicolour study of integrated luminosity of our targets, as well as of their surface brightness distributions could provide us with important clues to tackle the distinctive evolutionary properties of the galaxy population in the NGC 5044 group.

Again, our final results are collected in Table A1 and A2, respectively for the ESO and CASLEO observations.<sup>7</sup> In both tables, the total apparent magnitude (encircled within the  $\mu = 27 \text{ mag arcsec}^{-2}$  isophote in the  $g$  and  $V$  bands, respectively) is reported in col. 11, together with the mean surface brightness within the same isophotal radius, and within one effective radius (cols. 12 and 13, respectively) according to the corresponding values of  $\rho_{27}$  and  $\rho_e$ . Our output is finally completed with the  $griz$  colours (cols. 14 to 19 in

<sup>7</sup> In spite of the higher internal uncertainty (see Sec. 2), note that magnitudes and colours in Tables A1 and A2 are given with a nominal 3-digit precision simply for graphical purposes.

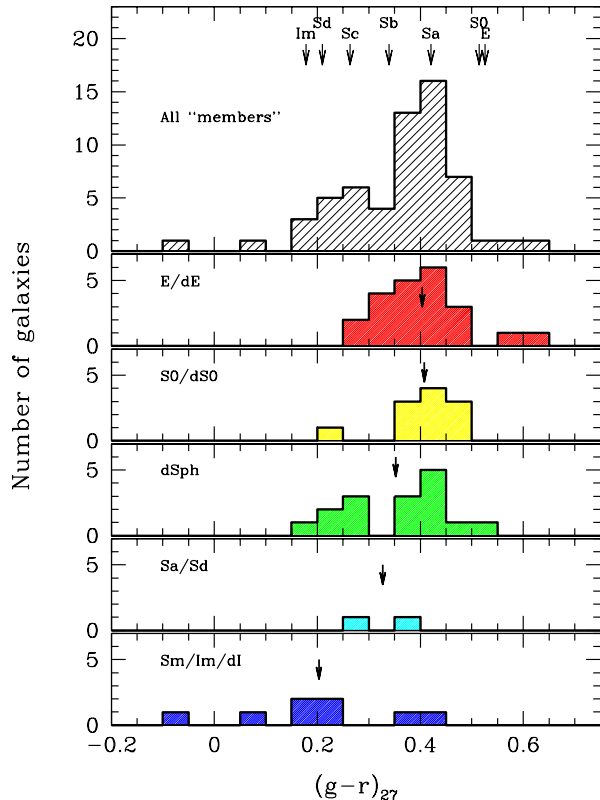


**Figure 5.** Apparent  $(g - r)$  colour distribution of ESO+CASLEO galaxy sample. Only likely members (“ $m_c$ ” code 1 and 2 of Table A1 and A2) are considered. These 59 galaxies (upper panel) are disaggregated in the different morphological groups along the different panels, as labelled. Mean colours as from the Buzzoni (2005) template galaxy models, matched to the observations according to Schlegel, Finkbeiner, & Davis (1998) reddening estimate, are marked on the top by small arrows. These are to be compared with the mean observed colours of each morphological class (as from Table 3), as marked (small arrows) in each panel.

Table A1) and  $(B - V)$  (cols. 14 and 15 in Table A2) across the same relevant apertures. Unless explicitly stated, note that no correction for Galactic reddening has been introduced. According to Burstein & Heiles (1982), the colour excess in the sky region around NGC 5044 amounts to  $E(g - r) \simeq E(B - V) \sim 0.03 \text{ mag}$ , a figure that may raise to  $\sim 0.07 \text{ mag}$  according to the Schlegel, Finkbeiner, & Davis (1998) reddening map.

#### 4.1 Colour and magnitude distribution

The colour distribution in the plane of integrated  $(g - r)$  for the whole sample of 59 “likely member” (membership code  $m_c \leq 2$  in Tables A1 and A2) galaxies with available colours is displayed in the upper panel of Fig. 5. In the other panels of the figure we also disaggregated the galaxy distribution according to homogenous morphology groups. Again, a clean overall trend can be recognized, with a colour shift from “red” to “blue” systems along the morphological sequence  $dE \rightarrow dS0 \rightarrow dSph \rightarrow Sabc \rightarrow dI$ . The mean colours, according to Table 3, are also marked in each panel, and consistently compare with the theoretical predictions from

**Table 3.** Mean observed colours for the ESO+CASLEO galaxy sample<sup>(a)</sup>

ESO+CASLEO sample		
Type	$\langle(g-r)\rangle^{(b)}$	no. of galaxies
dE	$0.401 \pm 0.082$	22
S0	$0.408 \pm 0.076$	11
dSph	$0.352 \pm 0.098$	16
Sa/Sd	$0.327 \pm 0.067$	2
Sm/Im	$0.203 \pm 0.167$	8
All	$0.360 \pm 0.118$	59

<sup>(a)</sup> Only likely member galaxies are considered (i.e. with membership code  $m_c \leq 2$  in Table A1 and A2). No correction for Galactic reddening has been applied.

<sup>(b)</sup> Mean colour within the  $\mu(g) \equiv 27$  mag arcsec<sup>-2</sup> isophote.

Buzzoni (2005) (the arrow sequence in the upper panel of the figure) once considering the reddening shift.

Whithin the whole colour distribution of Fig. 5, one has to notice the key location of dwarf spheroidals, largely overlapping the apparent colour range of spirals and ellipticals but with slightly bluer colours compared to S0 systems. Like for the Local Group counterparts (see, e.g. Tolstoy, Hill, & Tosi 2009, for an updated review), this feature actually accounts for the “bivalent” nature of these systems, bridging the morphological look of bulge-dominated systems and the composite photometric properties of disk-dominated galaxies, certainly reminiscent of a complex star formation history.

The galaxy distribution across the  $g$  vs.  $(g-r)$  c-m diagram is displayed in Fig. 6. The full sample (79 galaxies) has been plotted, marking however with solid symbols only the likely member galaxies (membership code  $m_c \leq 2$  in Tables A1 and A2). In order to reach a better sampling of the overall luminosity function of the cluster, we also picked up from the Ferguson & Sandage (1990) (50 galaxies) and Mendel et al. (2008) (46 galaxies) catalogs all the other likely or confirmed member galaxies (see Table 6 for their identification) not included in our observations. For these galaxies we converted the published  $B$  photometry into  $g$  magnitudes, according to our Table 2 calibration. As no direct colour information is available for this subsample, we framed these galaxies in Fig. 6 together with the five CASLEO objects lacking  $(B-V)$  information.<sup>8</sup>

Once considering the extended sample of all the Ferguson & Sandage (1990) and Mendel et al. (2008) galaxies, the diagram shows an evident morphology/luminosity segregation within the different galaxy groups. As for the two leading systems (namely NGC 5044 itself, of type E, and the Sb spiral NGC 5054), the bright tail of the galaxy population actually consists of a balanced mix of standard spirals and ellipticals, while a prevailing S0 population appears at absolute  $g$  magnitudes around  $M(g) \sim -18 \pm 1.5$ . Dwarf ellipticals follow at fainter magnitudes, sharing the

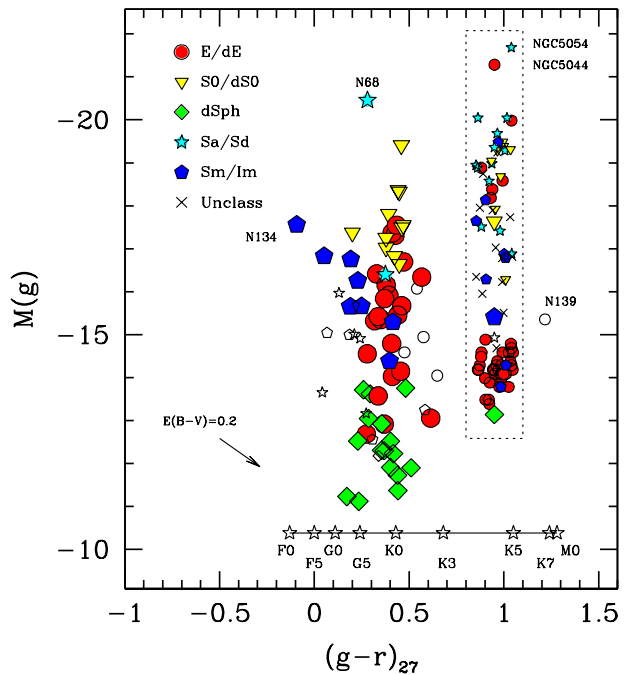


**Figure 6.** colour-magnitude diagram for the 74 galaxies of the ESO+CASLEO sample with available  $(g-r)$  or  $(B-V)$  colour. Solid markers refer to the likely group members (membership code  $m_c \leq 2$  in Table A1 and A2). A supplementary set of five CASLEO galaxies from Table A2, plus 50 likely member galaxies from the Ferguson & Sandage (1990) original catalog, and 46 supplementary members from the Mendel et al. (2008) survey, all lacking the colour information, have been added within the dotted box (with little random scatter for better reading) by converting  $V$  or  $B$  to  $g$  magnitudes via Table 2 calibration (see, in addition, footnote 8). A distance modulus  $(m-M) = 32.58$  mag has been adopted to obtain absolute  $g$  magnitudes. No correction for Galactic reddening has been applied to the data; the reddening vector is however reported bottom left in the plot. Photometric errors on  $(g-r)$  colours are between  $\sigma(g-r) \sim 0.04$  and  $0.06$  mag along the spanned magnitude range. Some outstanding objects, discussed in the text, are singled out and labelled. Star markers in the bottom line indicate the reference colours for stars of different spectral type, according to Straižys & Sviderskiene (1972), as labelled.

bulk of the galaxy population at intermediate luminosity ( $M(g) \sim -15 \pm 2$ ) with dwarf irregulars. Definitely, the low-luminosity tail of galaxy distribution coincides with a bunch of dwarf spheroidals, by definition, all fainter than  $M(g) \gtrsim -14$  and also standing out for their extremely low surface brightness ( $\mu_0(g) \gtrsim 25$  mag arcsec<sup>-2</sup>, see Fig. 4). The dSph’s clearly extend the colour-magnitude relation traced by early-type members down to  $M(g) \approx -11$ , with a scatter that is just mildly larger (likely due to their larger photometric errors) than the scatter at brighter magnitudes (see Smith Castelli et al. 2011, for an in-depth discussion on this topic).

Just on the basis of their location in the c-m diagram of Fig. 6, it is interesting to note that most of the “possible” ( $m_c = 3$  entries in Table A1 and A2) group members might in fact genuinely belong to the system. If confirmed by spectroscopy, then the dE/Im/dSph component of the cluster could even further increase. However, this can certainly

<sup>8</sup> For magnitude transformation of CASLEO, Ferguson & Sandage (1990) and Mendel et al. (2008) galaxies we adopted a reference  $(B-V) \sim 0.8 \pm 0.3$ . This reflects into a  $g$  magnitude uncertainty of roughly 0.3 mag in the framed points of Fig. 6.



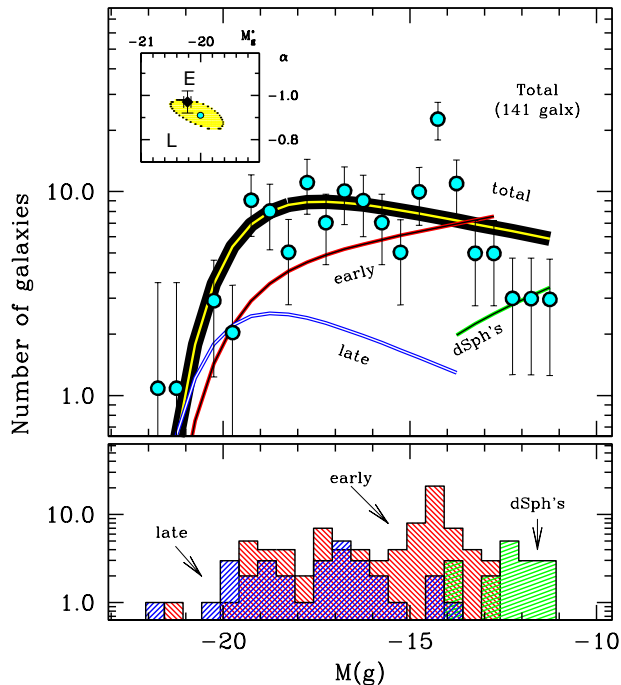


**Figure 7.** *Upper panel* - The  $g$ -band luminosity function for the 141 *bona fide* member galaxies (namely 59 objects from the present study, as from Table 3 plus 50  $m_c \leq 2$  members from Ferguson & Sandage (1990) plus 32 spectroscopically confirmed members from Mendel et al. (2008) with available  $B$  photometry. The thick solid line is the Schechter function for the global sample, according to the STY method of Sandage, Tammann, & Yahil (1979). An arbitrary normalization factor has been applied to the curve such as to rescale to the observed 141 galaxies. The global  $\alpha - M_g^*$  fitting parameters, together with their  $1\sigma$  confidence ellipse are also reported in the top left inset, comparing with the Zandivarez & Martinez (2011) general figures from the SDSS data (big diamond with error bars). The nominal fitting parameters for our early- and late-type galaxy subsamples are also marked in the plot with letters “E” and “L”, respectively. *Lower panel* - The total luminosity distribution is split into the three main components of early- (E+S0), late-type (Sa-Im) systems, and in the dSph component as well, as labelled. Note that the bright tail of the galaxy population actually consists of a balanced mix of standard spirals and ellipticals while dEs and dSph prevail at the faint-end tail of the magnitude distribution. For the sake of reference, the nominal Schechter fit for each of these subsamples, according to the previous STY procedure, is reported in the upper panel, as labelled.

not be the case for galaxy N139, a clear outlier in the plot and more likely a background standard elliptical placed at  $z \simeq 0.35$  according to its expected  $k$ -corrected colours (e.g. Buzzoni 1995).

The distinctive features about the group galaxy population more clearly emerge as far as the whole population of 141 *bona fide* member galaxies is considered to build up the group luminosity function, as displayed in Fig. 7. The tick solid line in the upper panel of the figure represents the global Schechter (1976) fit derived with the STY method (Sandage, Tammann, & Yahil 1979). This leads to a value for the estimated parameters of

$$[M_g^*, \alpha] = [-20.00_{-0.52}^{+0.39}, -0.91_{-0.07}^{+0.06}]. \quad (2)$$

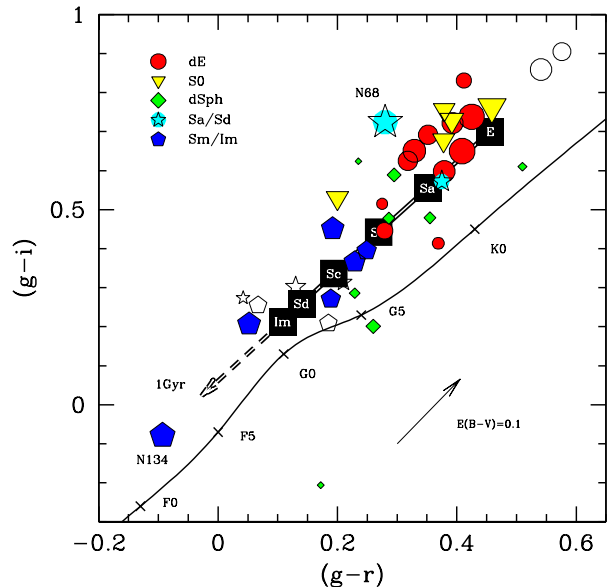


**Figure 8.** The  $(g-r)$  vs.  $(g-i)$  colour diagram for the 40 galaxies in the ESO sample. Likely group members (“ $m_c$ ” class 1 and 2 of Table A1 and A2) have been singled out as solid markers. Big solid squares indicate the expected colours for the 15 Gyr Buzzoni (2005) template galaxy models, as labelled. For the Im model, the dashed arrow traces the back-in-time colour evolution up to an age of 1 Gyr. The solid curve marks the reference locus for stars of different spectral type, as labelled, according to Straizys & Sviderskiene (1972). Data have not been corrected for Galactic reddening; the reddening vector is however reported bottom right in the plot. See text for a full discussion. Representative error bars for the data are of the order of the biggest marker size.

As a guideline, the nominal fits to the early- and late-type galaxy populations, as well as to the dSph component are also added to the panel, although within a much larger formal uncertainty, given the lower sample size.

The Schechter parameters derived for the total sample are well in agreement with the results of Zandivarez & Martinez (2011), who derived the luminosity function of galaxies in groups from the SDSS Data Release 7. In their work, these authors report the multicolour Schechter parameters for groups of different mass. After converting their  $^{0.1}g_{AB}$  SDSS magnitudes in the appropriate mass range to our magnitude system, according to Blanton & Roweis (2007), and rescaling consistently to our  $H_0$  value, we obtain

$$[M_g^*, \alpha]_{\text{SDSS}} = [-20.22 \pm 0.06, -0.97 \pm 0.05], \quad (3)$$

in fairly good agreement (within  $1\sigma$ ) with our result. The main contribution to the bright end of the luminosity function comes from standard spirals and ellipticals, while dEs and dSphs dominate the faint-end tail.

An additional view of the distinctive spectrophotometric properties of the galaxy population, although restrained to the 40 galaxies of the ESO sample, can be gained through a two-colour diagnostic, like the  $(g-r)$  vs.  $(g-i)$  diagram of Fig. 8. The galaxy distribution, according to the different morphological types, is compared with the Buzzoni (2005) template galaxy models and with the empirical stellar locus as derived from the Vilnius spectral catalog

**Table 4.** Theoretical colours and star formation parameters for the Buzzoni (2005) template galaxy models<sup>(a)</sup>

Morph. Type	$(B - V)$	$(B - K)$	$(g - r)$	$b^{(b)}$	M/L(B)	M/L(V) [ $M_{\odot}/L_{\odot}$ ]	M/L(g)
E	0.919	4.140	0.456	0.0	17.87	14.08	10.17
S0	0.908	4.077	0.444	0.0	16.47	13.11	9.49
Sa	0.762	3.774	0.351	0.2	10.08	9.18	6.82
Sb	0.649	3.455	0.269	0.5	6.07	6.13	4.66
Sc	0.555	3.188	0.194	0.9	3.33	3.67	2.84
Sd	0.493	2.990	0.140	1.3	1.77	2.06	1.62
Im	0.457	2.876	0.108	1.8	1.08	1.30	1.03

<sup>(a)</sup> At the reference age of 15 Gyr<sup>(b)</sup> Birthrate,  $b = \text{SFR}_0 / \langle \text{SFR} \rangle$ .

(Straizys & Sviderskiene 1972). Again, only likely members are plotted with solid markers. As expected, galaxies univocally discriminate with respect to stars displaying a “redder”  $(g - i)$  colour for fixed value of  $(g - r)$  (due to the red-giant stellar component contributing to the galaxy SED). Early-type galaxies (both dEs and S0s) fairly well match the Buzzoni (2005) theoretical locus for ellipticals, although displaying slightly bluer colours, as expected by their lower mass compared to “standard” systems (the same effect can also be easily recognized in the histograms of Fig. 5). In a few cases, however, the excursion toward even bluer colours, more appropriate to intermediate-type spirals, makes evident some star-formation activity among the dEs of lowest mass. Direct evidence in this sense has been collected for N50 (Cellone & Buzzoni 2001) displaying several blue knotty regions around its core. This may also be the case for N55, N93C, and N138, among the faintest dwarf ellipticals easily recognized also in Fig. 6 as “embedded” in the dSph region of the c-m diagram. Similarly, the case of N42, a relatively bright S0, seems worth of special attention for its exceedingly blue colours (see next section on this regard, and Cellone et al. 2011, in preparation, for an in-depth spectral analysis of this galaxy).

As far as the “magellanic” galaxy component (namely types Sm/Im) is concerned, one has to report its large colour spread in Fig. 8, a feature that clearly calls for a wide range of star-formation scenarios. The striking case of galaxy N134, the bluest and brightest ( $M(g) \sim -17.5$ ) object within this group, is worth of mention in this regard. Its colours are consistent with those of F-type stars, a feature that calls for a very young ( $t \ll 1$  Gyr) age, when compared with template galaxy models of this morphology. N134 lies at 2.6 arcmin ( $\sim 25$  kpc) projected distance from the centre of NGC 5054, partially overlapping the north arm of this luminous three-armed spiral. One could guess that the likely interaction between both galaxies may be the trigger for the intense star forming activity in N134; whether or not this interaction is also responsible for the peculiar arm morphology of NGC 5054 may still be matter of debate (e.g. Sandage & Bedke 1994; Eskridge et al. 2002).

In spite of the fairly bunched distribution in the c-m diagram, the population of dSphs stands out in Fig. 8 for its extreme colour spread, that largely encompasses the full theoretical locus for the different morphological types. Part of this peculiar distribution has certainly to be advocated to the large photometric uncertainties, given the very faint magnitude of these galaxies. The low mass of these systems also makes the integrated colours to be more easily biased

by a few outstanding stars inside each galaxy, consequent to fresh star formation. This may also give reason, for instance, of the bridging distribution of these galaxies across the stellar locus, as evident in Fig. 8. In any case, it is once more confirmed the puzzling essence of dwarf spheroidals, as multifaceted stellar systems able to easily change their distinctive look such as to escape any obvious classification within the reference evolutionary framework.

## 4.2 Inferred mass distribution and stellar birthrate

As a further step in our analysis, one could take advantage of the accurate distance to the group (Cellone & Buzzoni 2005), and a full morphological and photometric characterization of its galaxy members, to try a direct estimate of galaxy stellar mass and therefrom assess other fundamental physical properties of the group as a whole, such as its total bright mass and current stellar birthrate.

This can be done by matching our observed galaxy magnitudes with the appropriate stellar  $M/L$  ratio, as proposed by theoretical models. For its better accuracy,  $g_{27}$  and  $V_{27}$  photometry has been taken as a reference for the ESO and CASLEO samples, respectively. Again, the Buzzoni (2005) models provide the set of relevant quantities, as summarized in Table 4. As we previously discussed, the dSph case is hard to fit within the canonical scenario of standard morphological types. However, according to the observed colour distribution for these galaxies (see, again Fig. 5 and 8) one could envisage a composite stellar population vaguely resembling that of Sb spirals.

To consistently scale Gunn magnitudes to solar units we assumed for the Sun a colour  $(V - g)_{\odot} = -0.14$  obtained by convolving a (Straizys & Sviderskiene 1972) spectrum for a G2V star with the relevant  $V$  and  $g$  filters. Recalling, in addition, that  $M(V)_{\odot} = +4.79$  and  $M(B)_{\odot} = +5.45$  (Portinari, Sommer-Larsen, & Tantalo 2004), then  $M(g)_{\odot} = +4.93$ . Apparent  $g$  magnitudes for our ESO galaxies eventually translate into  $\mathcal{L}_g$  solar luminosities as

$$\mathcal{L}_g = 10^{-0.4 [(g-32.58)-4.93]}, \quad (4)$$

while, for the CASLEO  $V$  magnitudes, we have

$$\mathcal{L}_V = 10^{-0.4 [(V-32.58)-4.79]}. \quad (5)$$

If one wants to further complete the sample with the supplementary *bona fide* member galaxies comprised in the Ferguson & Sandage (1990) and Mendel et al. (2008) catalogs, then from their  $B$  photometry we can write,

**Table 5.** Inferred stellar mass for the present galaxy sample<sup>(a)</sup>

ESO sample			CASLEO sample		
Name	T	$\log M_{\text{gal}}^*$	Name	T	$\log M_{\text{gal}}^*$
N17	0	9.76	N18	1	10.68
N20	-5	8.59	N19	9	8.25
N24	9	8.25	N29	-5	10.17
N30	-5	9.90	N38	-5	9.43
N31	10	8.49	N46A	-4	7.88
N32	0	10.71	N49A	-4	7.66
N34	-5	9.54	N51	0	9.78
N42	0	9.90	N53	-5	9.70
N49	10	8.72	N57	-5	8.81
N50	-5	9.92	N58	10	7.87
N54	10	8.69	N61	-4	7.97
N54A	-4	7.13	N63	0	10.47
N55	-5	8.15	N66	-5	9.48
N56	-4	8.13	N72A	-4	7.86
N62	-4	7.81	N76	-5	9.84
N64A	-4	7.86	N79	0	9.85
N68	2	10.99	N80	-5	8.40
N70	-5	9.12	N82	0	10.45
N70A	-4	7.40	N82A	-4	7.52
N71	-5	9.44	N94	0	10.15
N75	0	9.85	N94A	-4	7.73
N83	-5	9.34	N94B	-4	7.88
N83A	-4	7.65	N95	-5	9.07
N89	-5	9.11	N95A	-4	8.47
N93A	-4	8.09	N108	-5	9.34
N93B	-4	7.09	N116	-5	8.57
N93C	-5	8.05	N117	0	10.12
N134	9	9.01	N122	-5	9.31
N138	-5	8.80	N131	0	10.14
N153	0	10.07	N131A	-4	8.19
N155	2	9.37	N149	10	8.24
N156	10	8.25			

<sup>(a)</sup> Only likely member galaxies (code  $m_c \leq 2$  in Table A1 and A2) are considered. Galaxy stellar mass  $M_{\text{gal}}^*$  in solar units from the assumed  $M/L$  ratio and absolute  $g$  magnitude, according to eq. (7).

$$\mathcal{L}_B = 10^{-0.4 [(B-32.58)-5.45]}. \quad (6)$$

Galaxy bright mass simply follows either as

$$M_{\text{gal}}^* = \begin{cases} \left(\frac{M}{L_g}\right) \mathcal{L}_g \\ \left(\frac{M}{L_V}\right) \mathcal{L}_V \\ \left(\frac{M}{L_B}\right) \mathcal{L}_B \end{cases} \quad (7)$$

providing to chose the appropriate  $M/L$  ratio from Table 4 according to galaxy morphology.

The results of our exercise, for the 63 likely member galaxies (membership code  $m_c \leq 2$  in Tables A1 and A2) in our sample plus the Ferguson & Sandage (1990) and Mendel et al. (2008) extra sample (50+23 objects with available photometry and morphological classification) are reported in Table 5, and 6, respectively, where for each entry the nominal output of eq. (7) is displayed.<sup>9</sup> The  $M_{\text{gal}}^*$  distribution for the likely-member galaxy sample is displayed in Fig. 9 splitting the contribution of the different morphological classes in the vertical panel sequence. A sharp lower-mass cutoff is evident in the distribution with a definite lack of galaxies below  $10^7 M_{\odot}$  and with the  $M_{\text{gal}}^* \lesssim 10^8 M_{\odot}$  population almost uniquely consisting of dSph type. The mean

<sup>9</sup> For those Mendel et al. (2008) galaxies lacking  $B$  photometry, eq. (7) has still been used, relying on the observed  $K$  magnitude and an appropriate  $(B-K)$  colour, according to morphology, as from Table 4.

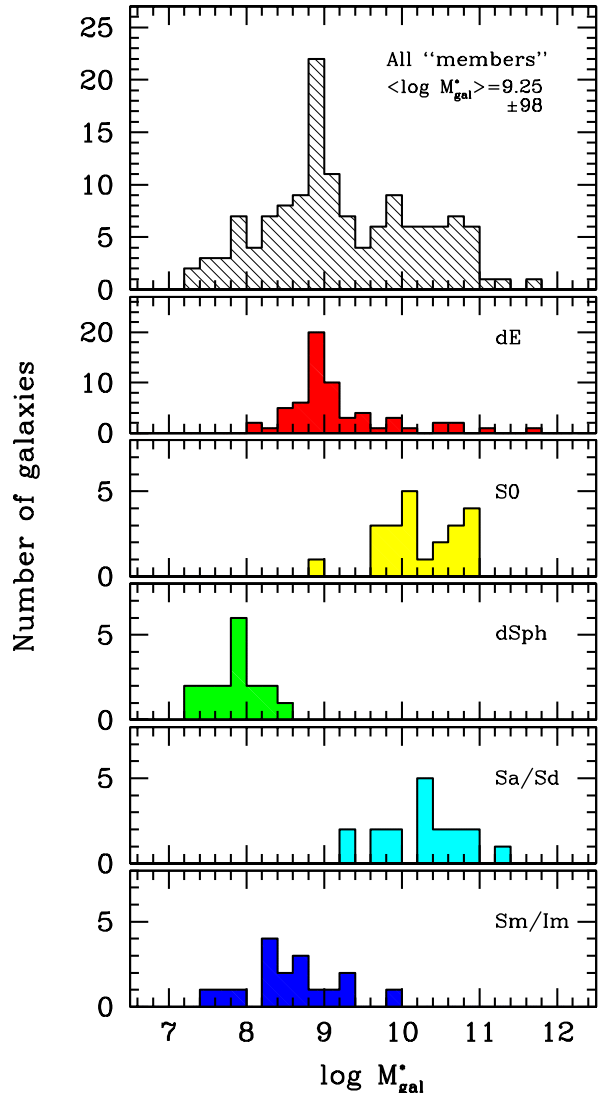


**Figure 9.** The bright stellar mass ( $M_{\text{gal}}^*$ ) of the 136 likely member galaxies with available photometry and morphological classification (63 from our sample, 50 more from the Ferguson & Sandage (1990) and 23 from the Mendel et al. (2008) catalogs), as inferred from the absolute  $g$ ,  $V$  or  $B$  luminosity and the theoretical  $M/L$  ratio as from the Buzzoni (2005) template galaxy models of Table 4. A mean logarithmic mass of  $\langle \log M_{\text{gal}}^* \rangle = 9.25 \pm 0.98$ , or  $\langle M_{\text{gal}}^* \rangle = 1.8 \cdot 10^9 M_{\odot}$  is derived for the whole sample, as reported in the top panel. The different morphological groups are singled out along the different panels, as labelled. Note a clear mass segregation effect, with systematically more massive dE’s and dS0’s galaxies compared to very low-mass dSph’s and Im’s.

logarithmic mass of the whole sample results  $\langle \log M_{\text{gal}}^* \rangle = 9.25 \pm 0.98$ , that is  $\langle M_{\text{gal}}^* \rangle = 1.8 \cdot 10^9 M_{\odot}$ , with galaxy mass spreading along nearly one order of magnitude.

A comparison with Mendel et al. (2009) can be attempted, by relying on the mass estimate for the 28 galaxies in common. For this set, these authors obtain a total of  $1.0 \cdot 10^{11} M_{\odot}$  versus our estimate of  $3.8 \cdot 10^{11} M_{\odot}$ , that is roughly a factor of four larger. This difference is mainly due to the adopted  $M/L$  ratio which, for Mendel et al. (2009),

**Table 6.** Inferred stellar mass for the supplementary set of confirmed member galaxies in the Ferguson & Sandage (1990) and Mendel et al. (2008) catalogs

Confirmed ( $m_c \leq 2$ ) members in Ferguson & Sandage (1990)				Confirmed members in Mendel et al. (2008) <sup>(a)</sup>				
Name	T	B	$\log M_{\text{gal}}^*$	Name	T	B <sup>(b)</sup>	K	$\log M_{\text{gal}}^*$
N1	-5	18.4	9.10	N3	3	14.3	9.34	10.28
N5	-5	13.2	11.18	N45	10	18.9	...	7.69
N7	-5	19.2	8.78	N69	-5	18.7	...	8.98
N9	0	14.5	10.63	N96	...	18.5	...	...
N11	0	18.9	8.87	N146	-5	19.1	...	8.82
N15	-5	14.6	10.62	N158	0	16.9	13.15	9.67
N16	10	19.4	7.49	2MASX:J13085477-1636106	...	16.37	12.97	...
N22	-5	18.9	8.90	2MASX:J13094408-1636077	0	13.87	9.75	10.88
N25	-5	19.0	8.86	2MASX:J13091671-1653115	...	16.40	12.83	...
N26	-5	18.9	8.90	2MASX:J13095347-1631018	0	<i>15.6:</i>	11.52	10.19
N27	4	14.2	10.32	2MASX:J13100952-1616458	...	17.23	12.34	...
N36	-5	19.1	8.82	2MASX:J13102493-1655578	...	13.94	10.11	...
N40	5	16.3	9.21	2MASX:J13114576-1915421	1	<i>13.2:</i>	9.44	10.94
N41	-5	18.8	8.94	2MASX:J13114703-1847312	4	15.67	12.93	9.73
N48	-5	19.7	8.58	2MASX:J13115849-1644541	...	15.29	11.96	...
N60	-5	18.9	8.90	2MASX:J13123543-1732326	5	13.14	8.85	10.48
N64	1	13.9	10.66	2MASX:J13133433-1525554	8	13.71	10.85	9.98
N67	-5	19.3	8.74	2MASX:J13143041-1732009	...	15.23	11.54	...
N72	0	13.9	10.87	2MASX:J13151278-1758006	7	14.61	12.32	9.62
N74	-5	19.4	8.70	2MASX:J13153736-1452209	...	...	11.24	...
N77	-5	19.7	8.58	2MASX:J13164875-1620397	...	15.45	11.60	...
N78	-5	15.0	10.46	2MASX:J13165533-1756417	0	15.26	11.94	10.32
N81	-5	19.1	8.82	MASX:J13171239-1715162	4	14.24	10.24	10.30
N84 <sup>(c)</sup>	-5	11.9	11.70	2MASX:J13182685-1545599	3	<i>15.0:</i>	11.57	...
N87	-5	19.1	8.82	2MASX:J13183034-1436319	5	<i>13.7:</i>	10.48	10.25
N91	-5	19.8	8.54	2MASX:J13184125-1904476	1	15.77	12.06	9.91
N97	-5	19.0	8.86	2MASX:J13185909-1835167	0	14.14	10.12	10.77
N100	-5	14.3	10.74	2MASX:J13191752-1509252	...	...	10.85	...
N102	0	13.7	10.95	2MASX:J13192062-1450402	5	13.14	9.16	10.48
N103	-5	19.2	8.78	2MASX:J13192221-1509232	...	...	13.16	...
N104	-5	18.9	8.90	2MASX:J13201698-1448455	...	...	11.33	...
N105	-5	19.0	8.86	2MASXi:J1320185-163215	...	14.44	11.13	...
N107	0	13.8	10.91	6dF:j1311150-180610	...	16.16	13.80	...
N112	-5	18.8	8.94	6dF:j1313501-173048	...	16.84	...	...
N113	-5	19.0	8.86	GEMS_N5044_5	...	...	...	...
N121	-5	18.6	9.02	GEMS_N5044_14	...	...	...	...
N123	-5	18.3	9.14	GEMS_N5044_7	...	17.68	13.62	...
N126	-5	19.1	8.82	GEMS_N5044_18	...	...	...	...
N127	-5	18.6	9.02	GEMS_N5044_1	...	...	...	...
N128	-5	19.0	8.86	PGC:045257	9	15.05	...	9.23
N133	-5	18.6	9.02	PGC:046242	...	16.96	...	...
N135	-5	18.6	9.02	PGC:046402	9	16.31	...	8.72
N137 <sup>(d)</sup>	3	11.5	11.40	PGC:046494	8	15.54	...	9.24
N141	5	13.5	10.33	HIPASS:J1312-15	...	...	...	...
N142	-5	18.5	9.06	HIPASS:J1320-14	...	...	...	...
N144	-5	14.8	10.54	FGC1563	8	16.4	13.23	8.90
N147	-5	19.2	8.78					
N151	-5	19.0	8.86					
N154	-5	19.4	8.70					
N162	9	16.9	8.49					

<sup>(a)</sup> This includes six entries originally classified as  $m_c = 3$  by Ferguson & Sandage (1990), whose membership has been spectroscopically confirmed, on the contrary, by Mendel et al. (2008).

<sup>(b)</sup> Entries in italics estimated from  $K$  magnitudes, according to the reference ( $B - K$ ) colour of theoretical templates from Table 4

<sup>(c)</sup> N84  $\equiv$  NGC 5044.

<sup>(d)</sup> N137  $\equiv$  NGC 5054.

Galaxy stellar mass  $M_{\text{gal}}^*$  in solar unit from the assumed  $M/L$  ratio and absolute  $B$  (or, in lack,  $K$ ) magnitude, according to eq. (7) and Table 4 colours.

comes from a plain SSP fitting of each galaxy, based on the Bruzual & Charlot (2003) population synthesis models. As stated by the authors, their procedure disregarded morphology details and star formation history, thus forcedly leading to younger “luminosity-weighted” ages for their galaxies (see Buzzoni 2011 and eq. 12 in Buzzoni 2005 for an estimate of this effect). In addition, the correspondingly lower  $M/L$  figures would be further decreased by the adopted Chabrier (2003) IMF. Compared to the Salpeter case, in fact, a Chabrier (2003) dwarf-depleted IMF leads to a brighter SSP

(and therefore to a lower  $M/L$  ratio) for fixed total stellar mass. According to our calculations, the total bright mass stored in the member galaxies of the group amounts to  $M_{\text{gal}}^*(\text{tot}) = \sum M_{\text{gal}}^* = 2.3 \cdot 10^{12} M_{\odot}$ , almost half of which being comprised in the three brightest members, that is NGC 5044 (22%), 5054 (11%) and the gorgeous Sab galaxy N68 (4%) (see CB05).

Based on the template galaxy models of Table 4, a nominal estimate of the current galaxy SFR for group mem-

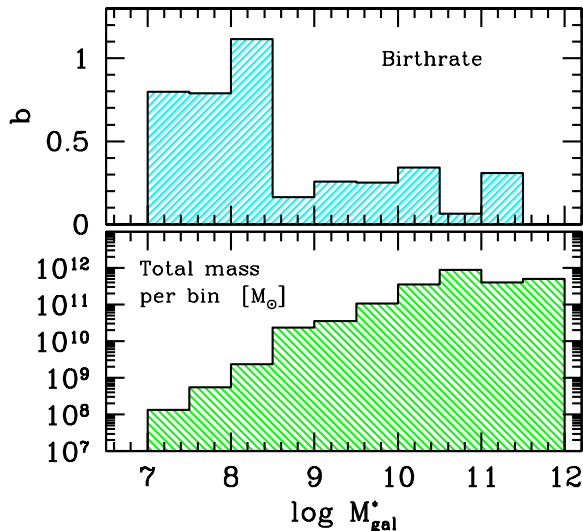


**Figure 10.** *Upper panel:* Mean birthrate versus galaxy stellar mass, as inferred from the match with the Buzzoni (2005) template galaxy models (see text for the detailed procedure). The total sample of the 136 likely-member galaxies of Fig. 9 is considered. Note the “downsizing” effect, with low-mass galaxies (of prevailing dSph/Im morphological type) supplying the fresh star formation within the NGC 5044 group. Fresh stars are produced inside the group at a rate of roughly  $23 M_{\odot} \text{ yr}^{-1}$ , while bright stellar mass sampled by our observations amounts to  $M_{\text{gal}}^*(\text{tot}) = \sum M_{\text{gal}}^* = 2.3 \cdot 10^{12} M_{\odot}$ . This total is singled out in the *lower panel* in terms of the cumulative galaxy mass fraction for each mass bin.

bers can even be guessed, through the model birthrate, i.e.  $b = \text{SFR}_0 / \langle \text{SFR} \rangle$ , so that

$$\text{SFR}_0 = \frac{b M_{\text{gal}}^*}{t_{\text{gal}}}, \quad (8)$$

being  $t_{\text{gal}}$  the assumed galaxy age. By summing up all the entries of Table 5 and 6 we have that fresh stars are produced inside the group at a rate of roughly  $23 M_{\odot} \text{ yr}^{-1}$ . Assuming galaxies to be one Hubble time old, in force of eq. (8) this leads to a global birthrate for the group of  $b_{\text{tot}} \simeq 0.15$ .

To much extent, such a low figure is mostly induced by the prevailing contribution of early-type galaxies among the more massive members of the NGC 5044 group (see the disaggregated distribution of Fig. 9). As a result, an important fraction of  $M_{\text{gal}}^*(\text{tot})$  resides in nearly quiescent stellar aggregates (see Fig. 10), while only very low-mass systems (mostly dSph and Im types) are still able to feed fresh stars to the global environment. Even at this small mass scale, therefore, the emerging picture seems consistent with the so-called down-sizing mechanism (Cowie et al. 1996; Gavazzi 1993), that is an inverse dependence of the birthrate with galaxy mass as the imposing paradigm for galaxy formation in the Universe.

## 5 SPECTROSCOPIC PROPERTIES

A preliminary analysis of the spectroscopic material collected along our survey has already been provided in Cellone & Buzzoni (2005, see Table 1 therein), where redshift measurements have been presented for 14 galaxies of

**Table 7.** Spectroscopic redshift for observed galaxies

Members			
ID	Type	cz [km s <sup>-1</sup> ]	Remarks
N17	0	2682	H $\beta$ emission
N29	-5	2351	from CASLEO
N30	-5	2411	
N34	-5	2661	
N42	0	2462	
N49	10	1499	
N50	-5	2392	H $\beta$ emission
N75	0	1831	
N84	-5	2710	NGC 5044 - H $\beta$ emission
N153	0	2816	
N155	2	2922	
Background			
ID	Type	z	Remarks
N109	8	0.018	
N33	5	0.045	
N152	7	0.045	H $\beta$ + [OIII] <sub>5007</sub> emission
N39	-5	0.091	
B1	-5?	0.097	
B3	-5	0.096	H $\beta$ + [OIII] <sub>5007</sub> emission
B2	-5?	0.282	
B4	>+5?	0.277	[OII] <sub>3727</sub> + H $\beta$ emission
B6	-5?	0.358	
B5	-5?	0.424	
Unclassified			
N20	-5	?	[OIII] <sub>5007</sub> emission?
N55	-5	?	
N156	10	?	

Galaxy type, in italics, refer to a spectroscopic classification alone.

the sample. For a total of 10 objects, the paper confirmed group membership, while 4 galaxies resulted to lie in the background. After thorough reconsideration of the data, also including the CASLEO observing sessions, we can further expand here the original output by including 7 more objects, for which a confident redshift measure can be obtained together with a rough morphological classification according to the detected spectral features. For a further set of 3 spectra no definite conclusions can be achieved, mostly due to the extremely poor S/N level. Our spectroscopic results, then, extend and complement the works of Mendel et al. (2008, 2009), which provided 103 (mostly new) redshifts for galaxies in the NGC 5044 Group catalog, as well as a stellar population analysis through Lick indices for a subset of 67 group members.

The summary of our results is presented in Table 7, which also recollects the data of Cellone & Buzzoni (2005) for reader’s better convenience. Out of the 25 objects considered by the observations, 10 galaxies, plus NGC 5044, belong to the same physical group, while behind one may guess the presence of at least three galaxy aggregations, that also match the Mendel et al. (2008) data, located respectively at  $z \sim 0.045, 0.095$ , and  $0.28$ , the farthest one actually confirmed by the coherent X-ray emission studied by XMM-Newton (Gastaldello et al. 2007a). The most distant galaxy in our sample is object B5, located at  $z = 0.42$ . According to Table 7, a roughly similar fraction of member and background galaxies is not a surprising feature, of course, given our observing strategy, that included a “bonus” object for each target pointing, as explained in Sec. 2.2. In this regard we stress the very high reliability of morphological membership assignment by Ferguson & Sandage (1990), which reaches  $\sim 91\%$  for  $m_c = 1$  galaxies (Mendel et al. 2008). As

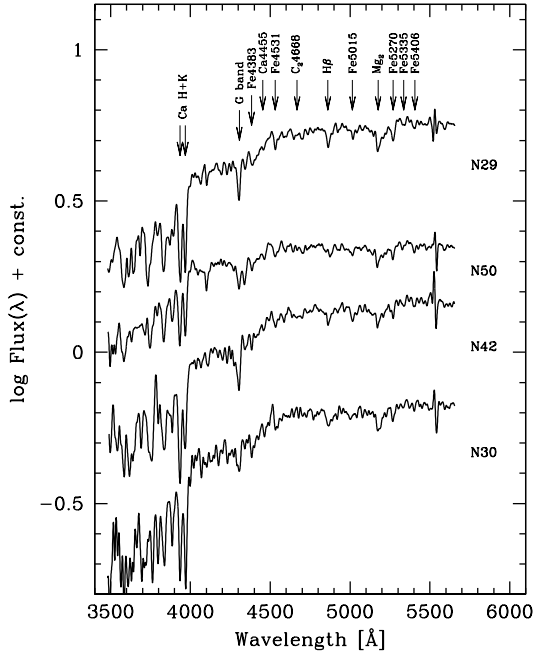


**Figure 11.** Spectral energy distribution for the four galaxies observed at CASLEO. For better reading, spectra have been degraded here to a resolution of 12 Å FWHM and corrected for redshift. The Ca H+K absorption lines together with all the main spectral features included in the Lick narrow-band index system (see Table 8) are marked on the top.

a reference for possible future investigations, we report in Table A4 the accurate coordinates for the 6 “B” galaxies caught by the spectrograph slit<sup>10</sup>

A graphical display of the SED for the 11 member galaxies is given in the series of Fig. 11 to 13. The CASLEO observations, obtained with a “bluer” setup are reported first in Fig. 11, while the ESO spectra are collected in the other two figures. For a closer “quick-look” analysis of the two data sets, and to increase S/N in the plots, all the displayed spectra have been homogeneously degraded to a FWHM resolution of 12 Å. Once comparing the three objects in common between ESO and CASLEO (namely galaxies N30, N42, and N50, as in Fig. 11 and 12) one sees that along the wavelength region in common the spectral pattern of absorption features is consistently reproduced in both data sets.

Some difference can be noticed, on the contrary, for the overall slope of the continuum emission. One has to consider, in this regard, that CASLEO spectra have all been taken at fixed (E/W) slit position angle; this is not the case for the ESO spectra for which a range of slit inclinations led in some cases to a larger departure from the parallactic angle, and therefore to a slightly poorer flux calibration. This effect has been explored by means of repeated spectra for the dE galaxy N34 taken in different nights. On the basis of the observed drift in the continuum shape we estimate that the induced internal uncertainty of our flux calibration can be quantified in  $\sim 10\%$ .

<sup>10</sup> Note that these coordinates update and complete the corresponding table originally proposed in Cellone & Buzzoni (2005).

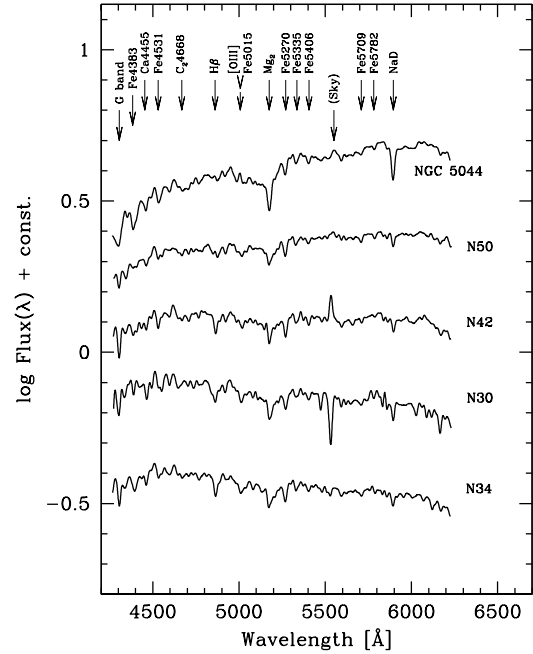


**Figure 12.** Same as Fig. 11, but for a first set of member galaxies observed at ESO including N50, N42 and N30 in common with CASLEO. For better reading, spectra have been degraded here to a resolution of 12 Å FWHM and corrected for redshift. Marked on the top are also all the main spectral features included in the Lick narrow-band index system (see Table 8).

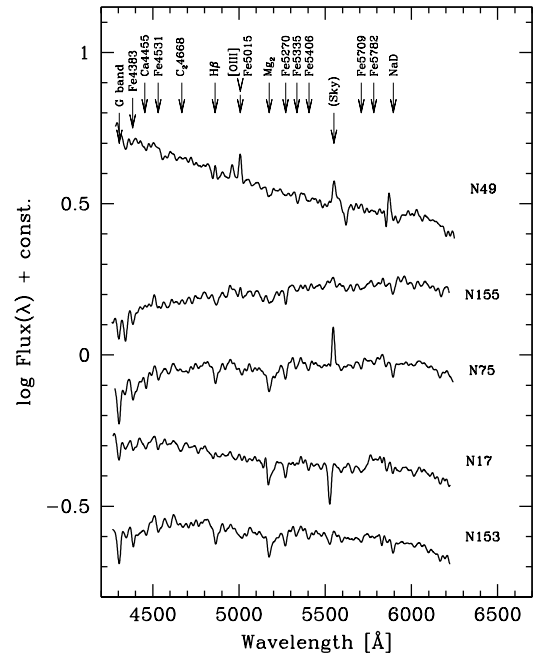


**Figure 13.** Same as Fig. 11, but for a second set of member galaxies observed at ESO. Note the outstanding Hβ and [OIII] 5007Å emission in Im galaxy N49. For better reading, spectra have been degraded here to a resolution of 12 Å FWHM, and corrected for redshift. Marked on the top are also all the main spectral features included in the Lick narrow-band index system (see Table 8).

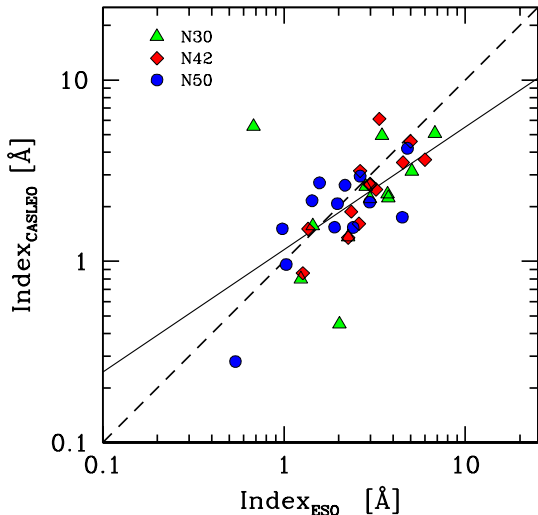


**Figure 14.** The set of Lick indices of Table 8 for the three galaxies in common between ESO and CASLEO observations (namely, N30, N42, and N50). Due to a poorer spectral resolution (10 Å FWHM), the CASLEO spectra show slightly “shallower” spectral features (and correspondingly lower indices) compared to the ESO spectra, better close to the Lick standard system. The dashed line in the plot is the one-to-one relation while the solid line is the least-squares fit of the points according to eq. (9). For better self-consistency, magnitude indices, like  $Mg_1$  and  $Mg_2$ , have been converted to pseudo-equivalent widths, as explained in the Footnote 11.

Concerning the background galaxy population, object B3 is probably the most striking case as the object is well resolved in our images, in spite of its relatively large redshift, and therefore was included in our photometry (see Table A1 and A2). Its Sérsic index ( $n = 0.22$ ) corresponds to a profile steeper than a de Vaucouleurs law, while the spectrum revealed an active elliptical with strong  $H\beta$  and  $[OIII]_{5007}$  line emission.

## 5.1 Lick Indices

In addition to the redshift information, the good spectroscopic material allowed us to tackle in finer detail the study of spectral properties of member and background galaxies in our sample. In particular, spectral resolution of both the ESO and CASLEO observations closely matched the canonical prescription (i.e.  $\sim 8$  Å FWHM) to consistently reproduce the Lick system (Worthey et al. 1994), thus allowing a wide set of narrow-band indices to be easily computed from the original data.

As for the ESO observations, our calculations have been carried out after slightly degrading the spectra to the Lick resolution by convolution with a Gaussian kernel. This transformation cannot be carried out with equivalent accuracy for the CASLEO data. Given their slightly poorer resolution (10 Å FWHM), in fact, these spectra tend to display shallower spectral features, and therefore lower index strengths. The effect can be assessed by means of Fig. 14 for the three galaxies in common between ESO and CASLEO spectra. The least-squares fit to the data indicates that the

corresponding indices (in Å pseudo-equivalent width) relate as<sup>11</sup>

$$\log(I_{\text{CAS}}) = \begin{matrix} 0.67 \log(I_{\text{ESO}}) & +0.06 \\ \pm 0.15 & \pm 0.07 \end{matrix} \quad (9)$$

with  $\rho = 0.60$  and  $\sigma = 0.22$ .

Although the lack of Lick primary calibrators in our sample prevented us to fully standardize our index scale, nevertheless a direct comparison can be done of our output for NGC 5044 itself with two reference sources in the literature, namely the work of Trager et al. (1998) and Annibali et al. (2006). As shown in Fig. 15, in both cases the index correlation is quite good ( $[\rho, \sigma] = [0.96, 0.13]$  with Trager’s data in the log-log index domain and  $[\rho, \sigma] = [0.91, 0.15]$  with the Annibali’s ones) assuring that the Lick standard system is correctly reproduced, on average, by our observations. Table 8 gives a general summary of our results.

### 5.1.1 $H\beta$ versus Magnesium

An instructive view can be gained for the NGC 5044 group (and its surrounding background galaxies) in the Lick-index domain. The Magnesium  $Mg_2$  index, together with the Balmer  $H\beta$  strength are certainly among the most popular reference tracers for this kind of analysis for their better dependence on metallicity ( $Mg_2$ ) and age ( $H\beta$ ), as extensively studied in the literature (see, e.g. Gorgas, Efstathiou, & Aragon Salamanca 1990; Buzzoni 1995; Thomas, Maraston, & Bender 2003; Tantalo & Chiosi 2004, for a discussion). The distribution of our sample is displayed in Fig. 16, comparing with the theoretical expectations for simple stellar population models (Buzzoni, Gariboldi, & Mantegazza 1992; Buzzoni, Mantegazza, & Gariboldi 1994) along an age range between 5 and 15 Gyr, and with metallicity spanning the interval  $-1.3 \leq [Fe/H] \leq +0.25$ . The sample of 50 old M31 and Galactic globular clusters, and 370 standard ellipticals from the work of Trager et al. (1998) is also superposed to the plot, together with a supplementary sample of 108 ellipticals with mild emission lines from Rampazzo et al. (2005) and Annibali et al. (2006) for a differential comparison with the distribution of high-mass systems likely experiencing some moderate star-formation activity. As a guideline for the distribution of young (metal-poor) stellar systems, we also added to the plot the sample of 14 globular clusters belonging to the Magellanic Cloud systems, according to de Freitas Pacheco, Barbuy, & Idiart (1998).

As expected, the  $Mg_2$ - $H\beta$  diagnostic is very poor for late-type galaxies, for which the  $H\beta$  index is strongly affected by gas emission; the location of the Im galaxy N49 in the plot is illustrative in this sense, once considering its strong spectral emission, as in Fig. 13. As far as the early-type galaxy component is concerned, however, one has to remark a pretty clean distribution of our dE+dS0 sample,

<sup>11</sup> To ease the comparison, in Fig. 14 and eq. (9) both  $Mg_1$  and  $Mg_2$  indices have been transformed from their magnitude scale to pseudo-equivalent width recalling that, by definition,  $I_{\Delta}^* = \Delta(1 - 10^{-0.4 I_{\text{mag}}})$ , being  $\Delta$  the width of the feature window, according to the standard index definition (Worthey et al. 1994). Therefore, we have that  $\Delta = 65$  Å for  $Mg_1$  and 42.5 Å for  $Mg_2$ .

**Table 8.** Lick narrow-band indices

Name	Type	G 4300	Fe 4383	Ca 4455	Fe 4531	C <sub>2</sub> 4668	H $\beta$	Fe 5015	Mg <sub>1</sub>	Mg <sub>2</sub>	Mgb	Fe 5270	Fe 5335	Fe 5406	Fe 5709	Fe 5782	NaD
<b>ESO sample</b>																	
N17	0	3.22	0.78	0.60	2.16	1.88	0.07	1.22	0.016	0.138	3.44	2.27	1.77	1.48			0.38
							<i>(0.83)</i>										
N30	-5	3.48	0.68	2.26	3.77	4.47	1.44	5.08	0.064	0.189	2.82	2.99	2.02	1.24	0.61		1.78
N34	-5	2.47	3.37	1.66	2.44	4.23	2.34	4.91	0.054	0.166	2.73	3.19	2.02	1.18	0.71	0.72	1.85
N42	0	3.36	2.63	1.27	2.99	6.00	2.26	4.53	0.051	0.136	2.35	3.22	2.59	1.36	0.55	0.48	1.48
N49	10	-3.44	-0.82	0.25	-0.22	0.60	-0.29	1.12	0.001	0.072	1.89	0.39	1.43	0.95	-0.48	0.06	1.95
N50	-5	1.43	1.57	0.98	2.63	2.17	0.54	4.50	0.041	0.130	1.97	2.97	1.90	1.03	0.79	0.78	1.76
							<i>(1.68)</i>										
N75	0	5.08	5.06	1.58	2.45	4.37	1.95	4.88	0.055	0.171	2.69	3.13	2.54	1.57	1.00	0.58	1.92
N84	-5	3.72	4.51	1.07	3.36	5.84	0.04	4.14	0.160	0.286	4.60	2.83	1.94	1.29	0.54	0.66	4.76
							<i>(0.64)</i>										
N153	0	4.97	3.26	1.36	3.40	5.20	2.06	4.76	0.036	0.161	2.84	2.67	1.87	1.62	0.73	0.27	1.63
N155	2	1.88	3.55	0.09	1.99	0.93	1.35	2.76	0.034	0.090	0.79	2.45	1.40	1.06	0.67	0.56	2.14
<b>CASLEO sample</b>																	
N29	-5	4.95	4.19	0.77	2.88	4.08	2.06	3.78	0.042	0.154	2.50	3.44	1.72	1.42			
N30	-5	4.93	5.54	1.36	2.24		1.57	3.14	0.040	0.138	2.59	2.21	0.45	0.80			
N42	0	6.10	3.15	0.86	2.67	3.63	1.35	3.51	0.045	0.124	1.88	2.49	1.61	1.51			
N50	-5	2.16	2.71	1.51	2.95	2.63	0.28	1.75	0.026	0.113	2.08	2.12	1.54	0.96			
							<i>(0.78)</i>										
<b>Background galaxies</b>																	
N109	8	-0.69	4.42	-1.25	5.93	0.63	3.31	-2.76	0.052	0.071	2.63	4.27	2.91	1.17	0.69	-0.31	0.50
N33	5	3.96	0.65	1.27	-0.41	-8.28	1.30	-2.48	-0.006	0.116	1.07	0.22	0.34	0.22	1.06		
N152	7	-0.06	1.37	0.77	1.63	2.28	-1.91	4.70	0.053	0.103	0.17	1.42	-0.87	-0.06	0.37		
N39	-5	5.90	5.12	1.81	3.26	5.91	1.38	5.21	0.113	0.219	3.56	2.93	1.51	1.01	0.08		
B1	-5	3.96	2.68	0.59	0.43	6.20	1.75	1.69	0.065	0.177	3.43	4.43	0.96	0.48	0.63		
B3	-5	3.31	3.92	0.45	1.96	0.07	-4.38	8.27	0.082	0.167	3.50	2.54	0.98	1.19	-0.05		

fully intermediate between Magellanic globular clusters and standard ellipticals, and pointing to a low (sub-solar) metallicity and an old age, consistent with the Hubble time.

In the latter respect, however, a word of caution still imposes in our conclusions as even for these galaxies a somewhat peculiar H $\beta$  strength might be envisaged to a closer analysis of the individual spectra (see Fig. 17). NGC 5044 itself (alias N84 in our catalog classification) is certainly a case in this regard, displaying an evident emission component, likely related to residual star formation and/or to a low-luminosity AGN (see Gastaldello et al. 2009; Brough et al. 2007, and references therein), superposed to the H $\beta$  absorption bulk. The same pattern also appears in the spectra of galaxies N17 (dS0) and N50 (dE). For the latter object, in particular, a composite stellar population spanning a wide age range has been suggested by Cellone & Buzzoni (2001) from a thorough study of the galaxy surface brightness distribution. Allover, these data show that the presence of excited residual gas, triggered by fresh star formation, might be a somewhat pervasive condition marking the evolution of low-mass ellipticals even at present day.

A proper correction of the H $\beta$  index such as to single out the genuine stellar absorption has widely proved, in the past, to be not a simple task. A standard procedure has been devised by González (1993), relying on the parallel measurement of the [OIII]<sub>5007</sub> strength, taken as a “proxy” of the intrinsic H $\beta$  emission.<sup>12</sup> However, such a relationship has found controversial evidence in the literature (see Carrasco et al. 1995; Trager et al. 2000; Serven & Worthey

2010, for a range of opinions), as Hydrogen and Oxygen coupling might be not so univocally constrained within the ISM gaseous phase depending on the range of thermodynamical conditions (e.g. Osterbrok 1974). Galaxy N50 itself, in Fig. 17, provides an outstanding example in this sense, as its spiked H $\beta$  emission does not seem to be accompanied by any evident [OIII]<sub>5007</sub> counterpart. Further support on this line is offered by Mendel et al. (2009, see Fig. 14 therein).

As sketched in Fig. 17, only for the macroscopic case of elliptical galaxies N17, N50 (both in the ESO and CASLEO spectra), and N84 we eventually adopted a plain and very prudent correction procedure to the H $\beta$  index, by means of a spline fitting such as to remove *at least* the visible emission spike. The corrected galaxy points have been plotted in Fig. 16, while their resulting H $\beta$  index is reported in Table 8 as an italics entry. In any case, it is clear that any hidden residual emission would reduce the H $\beta$  strength thus leading to overestimate the galaxy age, especially in case of younger star-forming ellipticals.

### 5.1.2 Iron versus $\alpha$ -elements

Together with H $\beta$  and Mg<sub>2</sub>, the sub-set of Fe5270 and Fe5335 indices, tracing the FeI features close to the strong Mg absorption at 5170 Å, complete the bulk of popular indices extensively used in literature for galaxy diagnostic. In particular, while Mg<sub>2</sub> is naturally sensitive to the abundance of the  $\alpha$  elements, the FeI indices provide a complementary piece of information to probe the overall metallicity of a stellar population (Buzzoni, Bertone, & Chavez 2009).

As sometimes attempted in the past literature (e.g. Idiart & Pacheco 1995; Gorgas et al. 1997; Zhu, Blanton, & Moustakas 2010), a better display of the

<sup>12</sup> In case a significant equivalent width  $E_{[\text{OIII}]}$  could be appreciated for the [OIII]<sub>5007</sub> forbidden emission, then González (1993) suggested to enhance the observed value of H $\beta$  by  $\Delta H\beta = 0.7E_{[\text{OIII}]}$ .



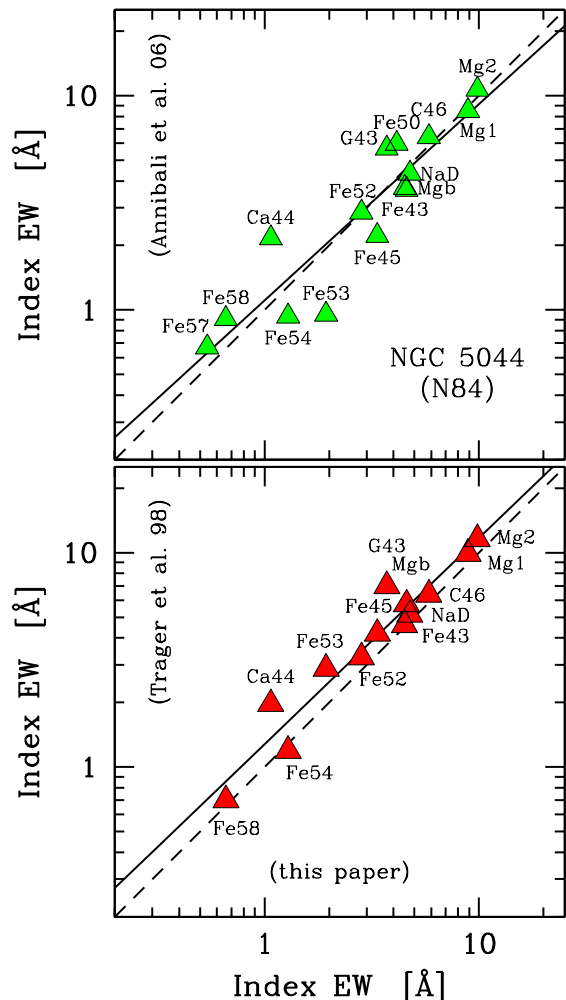


**Figure 15.** Lick-index comparison for NGC 5044. Our output from Table 8 is matched with two calibrated sources in the literature for the same galaxy. In particular, the observations of Annibali et al. (2006) are reported in the upper panel, while the data of Trager et al. (1998) are displayed in the lower panel, as labelled on the vertical axis.  $H\beta$  has been excluded in the plots being strongly affected by emission in this galaxy (see Fig. 17). Like Fig. 14, for dimensional self-consistency, the  $Mg_1$  and  $Mg_2$  magnitude indices have been converted here to pseudo-equivalent widths, as explained in the Footnote 11. Our data nicely correlate both with Annibali et al. (2006) ( $\rho = 0.91$ ) and with Trager et al. (1998) ( $\rho = 0.96$ ). The scatter of our index residuals, namely  $\sigma[\log(I_{\text{our}}/I_{\text{std}})]$ , with respect to the corresponding standard values amounts to  $\pm 0.15$  dex for Annibali et al. (2006) and  $\pm 0.13$  dex for Trager et al. (1998).

data can be done by averaging the two Fe features, like in a composite index

$$\langle Fe \rangle_2 = (Fe5270 + Fe5335)/2, \quad (10)$$

which actually sums up the equivalent width of both features.

An even cleaner result could also be secured for our dataset by taking advantage of the full observation of the 5 “Fe” indices comprised in the Lick system within the 4350–5406 Å range (see, again, Table 8), excluding the Fe5015 fea-

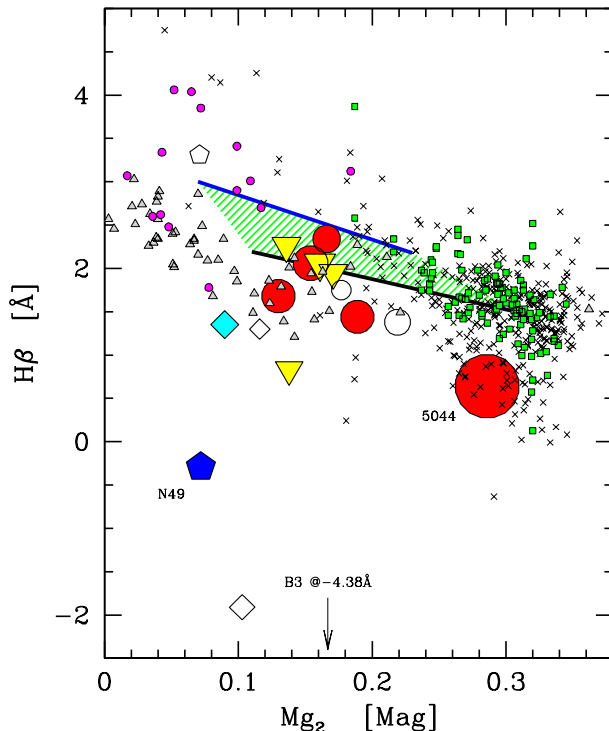


**Figure 16.** The Lick-gram of  $H\beta$  vs.  $Mg_2$  for the 16 ESO galaxies (10 members +6 background objects, the latter marked by open symbols) plus N29 from CASLEO. The small correction for  $H\beta$  emission has been applied to the index of N17, N50 and N84, as indicated in Table 8. Marker size is proportional to  $g$  luminosity, while morphological type is traced by different symbols, as in Fig. 6. The shaded region collects the theoretical SSP models of Buzzoni, Gariboldi, & Mantegazza (1992) and Buzzoni, Mantegazza, & Gariboldi (1994) for an age of 5 and 15 Gyr (upper and lower envelope, marked by thick solid lines), along the metallicity range  $-1.3 \leq [Fe/H] \leq +0.25$  (in the sense of increasing  $Mg_2$  values). The index distribution for the sample of 50 old M31 and Galactic globular cluster (small triangles) and 370 standard ellipticals (small crosses) from Trager et al. (1998) is also reported, for comparison, together with the group of 108 ellipticals with mild emission lines from Rampazzo et al. (2005) and Annibali et al. (2006) (heavy small squares) and 14 young globular clusters of the Magellanic Cloud, according to de Freitas Pacheco, Barbuy, & Idiart (1998) (small dots).

ture possibly affected in case of  $[OIII]_{5007}$  emission. A further composite index can therefore be built up as

$$\langle Fe \rangle_5 = (Fe4383 + Fe4531 + Fe5270 + Fe5335 + Fe5406)/5. \quad (11)$$

Figure 18 gives a summary of our results. Again, for reader’s better reference, our observed galaxy sample is matched in all the plots of the figure with the Rampazzo et al. (2005) and Annibali et al. (2006) standard ellipticals, as well as with the compilation of M31 and Galactic globulars according to Trager et al. (1998). The  $\langle Fe \rangle_2$  index can also be easily computed for the theoretical models of Buzzoni, Mantegazza, & Gariboldi (1994) and it is displayed in the upper plot of the figure as a reference locus for 10 Gyr old SSPs to compare with the observed distribution.

As for the standard ellipticals, even our dwarf early-type galaxies display a flat  $\langle Fe \rangle_2$  distribution vs.  $Mg_2$ .

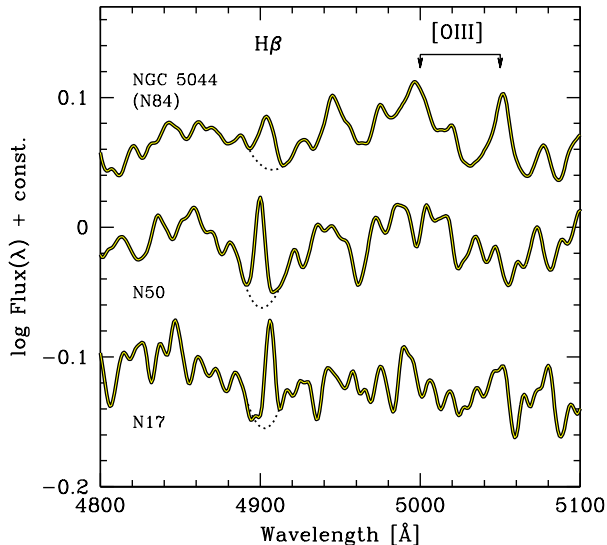


**Figure 17.** An  $H\beta$  gas emission component, superposed to the stellar absorption is clearly evident in the spectra of the three ellipticals NGC 5044 (alias N84), N50 and N17. Note, for the latter cases, that no sizeable [OIII] emission is detected at the expected (restframe) wavelength of 4959 and 5007 Å, as labelled. The envisaged (conservative) correction to  $H\beta$ , as explained in the text, is indicated here by the dashed curves.

This apparent decoupling between Iron and the other  $\alpha$  elements (as traced by Magnesium) is a well recognized feature (Gorgas, Efstathiou, & Aragon Salamanca 1990; Worthey, Faber, & Gonzalez 1992; Buzzoni, Mantegazza, & Gariboldi 1994), and probably the most direct evidence of the different enrichment channels that provided metals to the galaxies in the past. According to stellar evolution theory, in fact, we know that  $\alpha$ -elements are important yields for high-mass stars ( $M \gtrsim 8 M_{\odot}$ ) dying as Type II SNe; on the contrary, the Fe-Ni enrichment is more efficiently carried on by the Type Ia SNe, likely related to the binary-star environment. A steady trend of  $\langle Fe \rangle_2$  vs. Mg might therefore be resilient of a constant abundance of Iron, that is of a constant rate of Type Ia SNe (Buzzoni, Mantegazza, & Gariboldi 1994).

Apparently at odds with previous conclusions, however, the study of the  $\langle Fe \rangle_5$  meta-index reports a more explicit correlation between Fe and Mg along the entire mass range of standard and dwarf ellipticals. To a finer detail, this puzzling behaviour is mostly induced by a trend in place among the “bluer” Fe indices (namely Fe4383 and Fe4531). Contrary to the “red” indices (i.e. Fe5270, Fe5335 and Fe5406), when split into the different elemental contributions (see, for instance, Table 2 in Trager et al. 1998), all the “blue” indices are actually blends including an important presence of Ti and Mg, and this may eventually explain the apparent correlation between  $\langle Fe \rangle_5$  and  $Mg_2$ .

As a final remark dealing with Fig. 18, one has to note the somewhat unexpected general correlation of galaxy indices along the different morphological types. Although with larger individual uncertainties, in fact, also spirals and dwarf irregulars seem to obey in the plots the established relationship as for ellipticals. This interesting behaviour is largely in consequence of the much poorer (and similar) response of

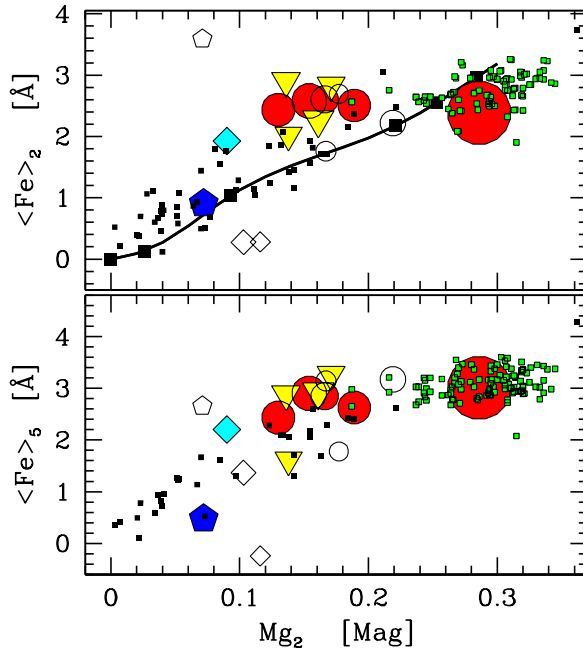


**Figure 18.** The Lick-gram of Iron meta-indices  $\langle Fe \rangle_2$  (upper panel) and  $\langle Fe \rangle_5$  (lower panel), as defined in the text (eq. 10, and 11) vs.  $Mg_2$  for the 16 ESO galaxies plus N29 from CASLEO. Symbols are as for Fig. 16. The SSP theoretical locus for  $t = 10$  Gyr, according to Buzzoni, Gariboldi, & Mantegazza (1992); Buzzoni, Mantegazza, & Gariboldi (1994), is displayed (solid curve in the upper panel), with the metallicity values marked up (solid squares) at  $[Fe/H] = -\infty, -2.3, -1.3, -0.25, \odot, +0.25$ , in the sense of increasing  $Mg_2$ . The index distribution for the Rampazzo et al. (2005) and Annibali et al. (2006) homogeneous sample of elliptical galaxies (small light squares) and the old M31 and Galactic globular clusters from Trager et al. (1998) (small dark squares) is also reported, for comparison.

both Mg and Fe indices to SSP age, that simply displaces their location in the plots along the SSP “universal” locus independently from the galaxy star-formation history.

### 5.1.3 The $\alpha$ - $\alpha$ element correlation

The natural correlation among  $\alpha$  elements within our galaxy sample can be verified by means of the two molecular features of Carbon, namely CH (alias G4300) and  $C_2$  at 4668 Å (see the two upper panels of Fig. 19), and the Calcium Ca4455 feature (as in the lower panel of the same figure). In both cases, a beautiful trend is in place with the NGC 5044 dwarf-galaxy population linking standard ellipticals with globular clusters. A slightly more scattered plot may be noticed for the G4300 index, however, perhaps in some cases affected by the influence of the closeby  $H\gamma$  emission.

Overall, one has also to report in the different panels of Fig. 18 and 19 a tendency for NGC 5044 itself to display slightly shallower absorption features compared to the expected strength for standard ellipticals of similar  $Mg_2$  value. We are inclined to ascribe this effect to the larger velocity dispersion of this galaxy, which is by far the most massive one of the group. The line broadening especially affects the shallowest features lowering the corresponding index strength. This is especially true, for instance, for the

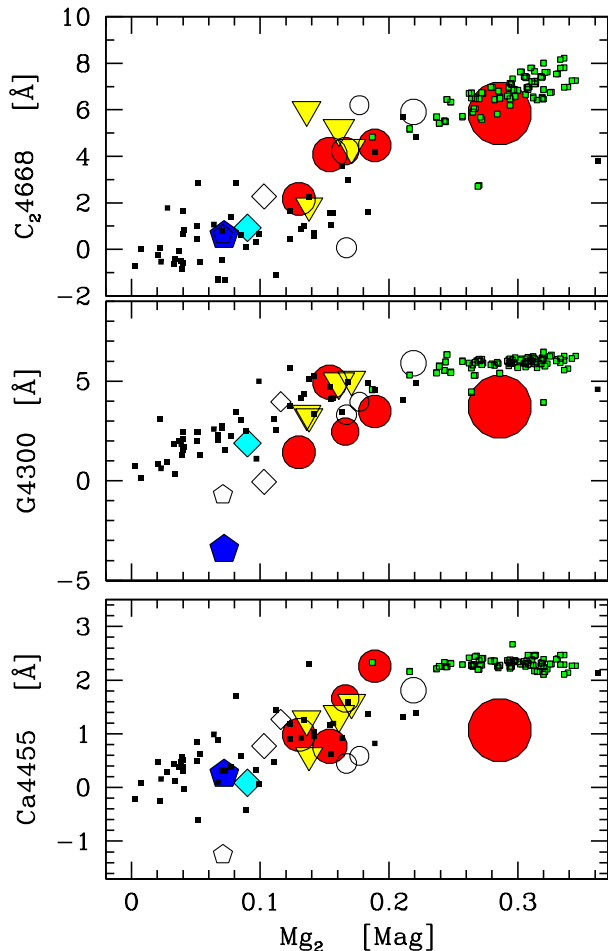


**Figure 19.** The Lick-gram for the two Carbon molecular indices  $C_2$  and CH (alias the G-band at 4300Å), and for the Calcium index Ca4455 vs.  $Mg_2$  for the 16 ESO galaxies plus N29 from CASLEO. Symbols are as for Fig. 16. The Rampazzo et al. (2005) and Annibali et al. (2006) galaxy sample is also overplotted, together with the M31 and Galactic globular clusters data of Trager et al. (1998) (small squares). See text for a full discussion.

Ca4455 feature, as displayed in Fig. 19. A hint in this sense also appears in Fig. 15, when comparing with the standard indices of Annibali et al. (2006) and Trager et al. (1998).

## 6 SUMMARY & CONCLUSIONS

With this third paper of a series (see also Cellone & Buzzoni 2001, 2005), we conclude our long-term project on the study of the galaxy group surrounding the standard elliptical NGC 5044. As widely recognized in the recent literature (Faltenbacher & Mathews 2005; Sengupta & Balasubramanyam 2006; Brough et al. 2006; Mendel et al. 2008, 2009) this group is an outstanding aggregate in the local Universe for its notable population of low-mass (both dwarf and LSB) galaxies, which take part in a massive ( $M_{\text{tot}} \sim 1.6 \cdot 10^{13} M_{\odot}$ , Betoya-Nonesca, Fukazawa, & Ohsugi 2006) dynamically relaxed structure, as traced by the diffuse X-ray emission of the group (Buote et al. 2003; Brough et al. 2006).

Along several observing runs carried out at the CASLEO (San Juan, Argentina) and ESO (La Silla, Chile) telescopes we collected multicolour  $B, g, V, r, i, z$  photometry for a significant fraction (79 objects) of the faintest galaxies projected on the NGC 5044 sky region assessing cluster membership on the basis of apparent morphological properties (through accurate Sérsic profile fitting) and low-resolution ( $R = 500 - 1000$ ) spectroscopy to estimate redshift for 25 objects in the field.

Both on the basis of the morphological and spectrophotometric properties of the member galaxies, it is evident from our analysis a marked segregation effect within the global population. As far as the galaxy surface-brightness profile is concerned, a clear separation can be made in the Sérsic parameter space between early- and late-type systems, the first showing in nearly all cases a “concave” (shape parameter  $n \lesssim 1$ ) radial brightness profile. Magellanic systems, on the contrary, stand out in the distribution for their clean exponential profile ( $n \simeq 1$ , see Fig. 3), while dwarf spheroidals confirm their sort of “acephalous” structure, where the “convex” profile ( $n > 1$ ) lacks of any nuclear design, and the galaxy body vanishes into a thin external envelope of extremely faint mean surface brightness ( $\mu(g) \gtrsim 26$  mag arcsec $^{-2}$ , see Fig. 4). Overall, compared with a de Vaucouleurs  $R^{1/4}$  profile, typical for standard ellipticals, the dwarf early-type galaxies in the group (dE, dS0, dSph) characterize for their “broader” (i.e. poorly-nucleated) surface-brightness distribution.

The intrinsically bluer colour and the larger colour spread, compared to the other morphological sub-groups (see, in particular, Fig. 5 and Table 3), marks the population of Magellanic irregulars, pointing to a wide range of star-formation histories. The case of the Sm galaxy N134 is a notable one in this regard, appearing to be the youngest member of the N5044 group with an age well less than 1 Gyr (see Fig. 8), probably as a result of its ongoing interaction with NGC 5054. On the other hand, a drift toward bluer integrated colours is also an issue for dE’s, a feature that may point to some moderate star-formation activity even among these nominally “quiescent” stellar systems (see, e.g. Cellone & Forte 1996, for similar results with the Fornax cluster dE’s).

Once rescaling for the group distance, the absolute magnitude distribution indicates that in the NGC 5044 group we are dealing with a prevailing fraction of systems fainter than  $1.8 \cdot 10^9 L_{\odot}$  (see Sec. 4.2). In particular, dwarf ellipticals and irregulars, together, mark the bulk of the galaxy population around  $M(g) \simeq -18.0 \pm 1.5$ , while dSph’s characterize the faint-end tail of the galaxy distribution (Fig. 6 and 7). The leading role of disk galaxies may even better impose when considering that, apart from NGC 5044 that leads the group as an elliptical, the other three brightest members (heading then the underlying dS0 line in the c-m diagram) are all spirals, namely NGC 5054 (type Sb), N68 (Sab) and N18 (Sab).

To some extent, this further emphasizes the quite special location of the NGC 5044 group, within the cosmic aggregation scale, being strategically placed just “midway” between the high-density environment of galaxy clusters, and the low-density conditions of looser galaxy clumps like our Local Group. Recalling the recent discussion of Gavazzi et al. (2010) about the “nurture” effects on galaxy

evolution, it is interesting to remark that this “duality” of the NGC 5044 group reflects also in the prevailing galaxy mix within the aggregate, where the gas-depleted population of dwarf ellipticals (a typical sign of dense cosmic environments) coexists with an important population of dwarf (gas-rich) irregulars (the typical inhabitants of low-density regions in the Universe).

A tentative assessment of the mass budget sampled by the group member galaxies has been carried out in Sec. 4.2 on the basis of the observed colours and the morphology of each object. By relying on the Buzzoni (2005) template models of Table 4, this combined piece of information allowed us to assign a representative M/L such as to convert absolute magnitudes into bright (baryonic) mass. Overall, the 63 member galaxies in our sample complemented by other 50 likely members comprised in the Ferguson & Sandage (1990) original catalog (which includes NGC 5044 and 5054 themselves), and by 23 additional member galaxies with available photometry and morphological type from the Mendel et al. (2008) survey (see Table 5 and 6) collect a total of  $M_{\text{tot}}^{\text{bright}} = 2.3 \cdot 10^{12} M_{\odot}$ , with a mean representative value of  $\langle \log M_{\text{gal}}^* \rangle = 9.2 \pm 1.0$  for the member galaxies (see Fig. 9). Roughly one fourth of  $M_{\text{tot}}^{\text{bright}}$  is stored in NGC 5044 itself, while the three brightest members, alone, represent nearly half the total bright mass of the group.

The derived total bright mass is about one seventh of the total dynamical mass of the group as inferred from the X-ray emission map. This fraction might however be getting even smaller if one accounts for a larger estimate between  $M_{\text{tot}}^{\text{dyn}} \sim 3.7 \cdot 10^{13} M_{\odot}$  (Gastaldello et al. 2007b) and  $9.9 \cdot 10^{13} M_{\odot}$ , according to Mendel et al. (2008), just on the basis of the galaxy velocity dispersion.

Like in the luminosity function, a clear morphological segregation is also in place for galaxy masses with dE and dS0 systems which surmount the Im and dSph component. The latter, in particular, constrains the low-mass tail of the mass function providing the key connection between galaxies and globular clusters, around the  $10^7$ - $10^8 M_{\odot}$  mass range. A more marked presence of later-type systems among the faintest galaxy population naturally complies with the downsizing mechanism (Gavazzi et al. 2010) making active star formation to better confine among low-mass aggregates, as shown in Fig. 10.

As discussed in Sec. 4, fresh stars are produced within the NGC 5044 group at a rate of roughly  $23 M_{\odot} \text{ yr}^{-1}$ , implying a global birthrate  $b \sim 0.15$ . This figure might however be a prudent lower limit, as it does not account for the contribution of the two brightest members of the group and for the possible star-forming activity even among dE and dS0 galaxies. Some evidence in this sense stems, in fact, from the broad colour spread of these galaxies in Fig. 8, but even clearer signs emerge from the spectroscopic analysis of Sec. 5. In particular, Fig. 17 shows that the general presence of H $\beta$  emission in the spectra of many dwarf ellipticals (and in NGC 5044 itself) is resilient of a moderate but pervasive activity of fresh star formation throughout in the group environment.

The good spectroscopic material, collected along the same photometric observing runs added a number of useful details to characterize the evolutionary status of the NGC 5044 group. These data allowed a univocal member-

ship classification in most ambiguous cases discriminating between genuine dwarf galaxies belonging to the group and bright background galaxies (see Table 7); the case of objects B3 and N39 is illustrative in this sense, as both ellipticals eventually resulted to be part of a background structure at  $z \sim 0.095$ . In this regard, at least three relevant galaxy aggregates appear beyond our group, the farthest one being a confirmed galaxy cluster at  $z \sim 0.28$  (Gastaldello et al. 2007a).

The resolution and wavelength coverage for ESO and CASLEO spectra also allowed us to self-consistently derive a series of Lick narrow-band indices, as summarized in Table 8. In particular, eight relevant features of Iron between 4300 and 5800 Å have been sampled, while  $\alpha$  elements can be traced by means of the 4455 Å Ca feature and the striking Mg feature at 5170 Å. In addition, two molecular bands of Carbon (CH at 4300 Å, and C<sub>2</sub> at 4668 Å) complete our diagnostic tools. As far as early-type galaxies are concerned, spectroscopic analysis clearly indicate for them a sub-solar metallicity ( $-1.0 \lesssim [Fe/H] \lesssim -0.5$ , see especially Fig. 18), and in general an old age, consistent with the Hubble time. In the latter respect, however, one has to be aware of the possible hidden bias (toward higher values) in age diagnostic via H $\beta$  absorption strength (Fig. 17) due to the effect of gas emission.

As for the established relationship for high-mass ellipticals (Worthey, Faber, & Gonzalez 1992), also the dwarf population of NGC 5044 shows a decoupled trend between Iron and  $\alpha$  elements (as in the upper panel of Fig. 18), consistent with the mild trend between  $[\alpha/Fe]$  and stellar mass for  $M > 10^{8.5} M_{\odot}$  galaxies shown by Mendel et al. (2009). This feature supports and further extends also to the low-mass framework the canonical picture for galaxy chemical evolution as a result of the two distinct enrichment channels dealing with Type I and Type II SNe (see, e.g. Matteucci & Greggio 1986).

## ACKNOWLEDGMENTS

We warmly thank ESO and CASLEO staffs for their skillful assistance. The anonymous referee is also acknowledged for several timely comments to the original draft. Funding from ANPCT (Argentina), PICT 03-00339 (1998) is also acknowledged. SAC would like to thank CONICET and UNLP for funding through personal grants, and the Astronomical Observatories of Brera-Merate and Bologna, Italy, for their hospitality. The Universidad Nacional de La Plata is also acknowledged by one of us (AB) for friendly and generous support along the many visits to Argentina in the framework of this project.

## REFERENCES

- Aloisi A., et al., 2007, ApJ, 667, L151
- Annibali F., Bressan A., Rampazzo R., Zeilinger W. W., 2006, A&A, 445, 79
- Arimoto N., 1995, ASPC, 86, 239
- Arimoto N., Tarrab I., 1990, A&A, 228, 6
- Baldwin J. A., Stone R. P. S., 1984, MNRAS, 206, 241

- Betoya-Nonesa J. G., Fukazawa Y., Ohsugi T., 2006, PASJ, 58, 103
- Binggeli B., Sandage A., Tammann G. A., 1985, AJ, 90, 1681
- Blanton M. R., Roweis S., 2007, AJ, 133, 734
- Brough, S., Proctor, R., Forbes, D. A., Couch, W. J., Collins, C. A., Burke, D. J., & Mann, R. G. 2007, MNRAS, 378, 1507
- Bothun G. D., Mould J. R., 1988, ApJ, 324, 123
- Brodie J. P., Huchra J. P., 1991, ApJ, 379, 157
- Brough S., Forbes D. A., Kilborn V. A., Couch W., 2006, MNRAS, 370, 1223
- Bruzual G., Charlot S., 2003, MNRAS, 344, 1000
- Buote D. A., Lewis A. D., Brighenti F., Mathews W. G., 2003, ApJ, 594, 741
- Burstein D., Heiles C., 1982, AJ, 87, 1165
- Buzzoni A., 1995, ApJS, 98, 69
- Buzzoni A., 2005, MNRAS, 361, 725
- Buzzoni A., 2011, MNRAS, 415, 1155
- Buzzoni A., Gariboldi G., Mantegazza L., 1992, AJ, 103, 1814
- Buzzoni A., Mantegazza L., Gariboldi G., 1994, AJ, 107, 513
- Buzzoni A., Bertone E., Chavez M., 2009, ApJ, 703, L127
- Campos P. E., Mendes de Oliveira C., Bolte M., 2004, Outskirts of Galaxy Clusters: Intense Life in the Suburbs. Eds. A. Diaferio, IAU Coll. #195, p.441
- Carrasco L., Buzzoni A., Salsa M., Recillas-Cruz E., 1995, Fresh views of elliptical galaxies. ASP Conf. Series, 86, eds. A. Buzzoni, A. Renzini, and A. Serrano (San Francisco: ASP), p.235
- Cellone S. A., 1999, A&A, 345, 403
- Cellone S. A., Buzzoni A., 2001, A&A, 369, 742
- Cellone S. A., Buzzoni A., 2005, MNRAS, 356, 41
- Cellone S. A., Buzzoni A., 2007, Groups of Galaxies in the Nearby Universe, 91
- Cellone S. A., Forte J. C., 1996, ApJ, 461, 176
- Cellone S. A., Forte J. C., Geisler D., 1994, ApJS, 93, 397
- Chabrier G., 2003, PASP, 115, 763
- Conselice C. J., Gallagher J. S., III, Wyse R. F. G., 2001, ApJ, 559, 791
- Cowie L. L., Songaila A., Hu E. M., 1991, Nature, 354, 460
- Cowie L. L., Songaila A., Hu E. M., Cohen J. G., 1996, AJ, 112, 839
- Davies J. I., Phillipps S., Cawson M. G. M., Disney M. J., Kibblewhite E. J., 1988, MNRAS, 232, 239
- Deady J. H., Boyce P. J., Phillipps S., Drinkwater M. J., Karick A., Jones J. B., Gregg M. D., Smith R. M., 2002, MNRAS, 336, 851
- de Freitas Pacheco J. A., Barbuy B., Idiart T., 1998, A&A, 332, 19
- Dressler A., 1980, ApJ, 236, 351
- Drinkwater M. J., Gregg M. D., Holman B. A., Brown M. J. I., 2001, MNRAS, 326, 1076
- Eskridge P. B., et al., 2002, ApJS, 143, 73
- Faltenbacher A., Mathews W. G., 2005, MNRAS, 362, 498
- Ferguson H. C., 1989, AJ, 98, 367
- Ferguson H. C., Binggeli B., 1994, A&AR, 6, 67
- Ferguson H. C., Sandage A., 1990, AJ, 100, 1
- Ferrarese L., et al., 2006, ApJS, 164, 334
- Forbes D. A., 2007, Groups of Galaxies in the Nearby Universe, eds. I. Saviane, V.D. Ivanov, J. Borissova, ESO Astrophys. Symp. (Heidelberg: Springer-Verlag), p. 97
- Gastaldello F., Buote D. A., Humphrey P. J., Zappacosta L., Seigar M. S., Barth A. J., Brighenti F., Mathews W. G., 2007a, ApJ, 662, 923
- Gastaldello F., Buote D. A., Humphrey P. J., Zappacosta L., Bullock J. S., Brighenti F., Mathews W. G., 2007b, ApJ, 669, 158
- Gastaldello F., Buote D. A., Temi P., Brighenti F., Mathews W. G., Etori S., 2009, ApJ, 693, 43
- Gavazzi G., 1993, ApJ, 419, 469
- Gavazzi G., Donati A., Cucciati O., Sabatini S., Boselli A., Davies J., Zibetti S., 2005, A&A, 430, 411
- Gavazzi G., Fumagalli M., Cucciati O., Boselli A., 2010, A&A, 517, A73
- González J. J., 1993, PhDT,
- Gorgas J., Efstathiou G., Aragon Salamanca A., 1990, MNRAS, 245, 217
- Gorgas J., Pedraz S., Guzman R., Cardiel N., Gonzalez J. J., 1997, ApJ, 481, L19
- Grebel E. K., 2005, Near-fields cosmology with dwarf elliptical galaxies, IAU Coll. 198, eds. Jerjen, H. & Binggeli, B. (Cambridge: Cambridge Univ. Press), p.1
- Gutiérrez-Moreno A., Moreno H., Cortés G., Wenderoth E., 1988, PASP, 100, 973
- Held E. V., 2005, Near-fields cosmology with dwarf elliptical galaxies, IAU Coll. 198, eds. Jerjen, H. & Binggeli, B. (Cambridge: Cambridge Univ. Press), p.11
- Held E. V., Mould J. R., 1994, AJ, 107, 1307
- Helsdon S. F., Ponman T. J., 2003, MNRAS, 339, L29
- Hilker M., Kissler-Patig M., Richtler T., Infante L., Quintana H., 1999, A&AS, 134, 59
- Ichikawa S.-I., Wakamatsu K.-I., Okamura S., 1986, ApJS, 60, 475
- Idiart T. P., Pacheco J. A. D. F., 1995, AJ, 109, 2218
- Jerjen H., Dressler A., 1997, A&AS, 124, 1
- Jerjen H., Kalnajs A., Binggeli B., 2000, A&A, 358, 845
- Jørgensen I. 1994, PASP, 106, 967
- Karachentseva V. E., Karachentsev I. D., Boerngen F., 1985, A&AS, 60, 213
- Kaufmann et al. 1993, MNRAS, 264, 201
- Kelm B., Focardi P., Sorrentino G., 2005, A&A, 442, 117
- Kent S. M., 1985, PASP, 97, 165
- Knezek P. M., Sembach K. R., Gallagher J. S., III, 1999, ApJ, 514, 119
- Kuzio de Naray R., McGaugh S. S., de Blok W. J. G., 2004, MNRAS, 355, 887
- Landolt A. U., 1992, AJ, 104, 340
- Lisker T., Grebel E. K., Binggeli B., Glatt K., 2007, ApJ, 660, 1186
- Maia M. A. G., da Costa L. N., 1990, ApJ, 352, 457
- Matteucci F., Greggio L., 1986, A&A, 154, 279
- Mendel J. T., Proctor R. N., Forbes D. A., Brough S., 2008, MNRAS, 389, 749
- Mendel J. T., Proctor R. N., Rasmussen J., Brough S., Forbes D. A., 2009, MNRAS, 396, 2103
- Mieske S., Hilker M., Infante L., 2004, A&A, 418, 445
- Osterbrok D. E., 1974, Astrophysics of Gaseous Nebulae and Active Galactic Nuclei. University Science Books, Mill Valley
- Paturel G., Petit C., Prugniel P., Theureau G., Rousseau J., Brouty M., Dubois P., Cambrésy L., 2003, A&A, 412,

45  
 Portinari L., Sommer-Larsen J., Tantalo R., 2004, MNRAS, 347, 691  
 Postman M., Geller M. J., 1984, ApJ, 281, 95  
 Rampazzo R., Annibali F., Bressan A., Longhetti M., Padoan F., Zeilinger W. W., 2005, A&A, 433, 497  
 Roberts S., et al., 2004, MNRAS, 352, 478  
 Sabatini S., Davies J., van Driel W., Baes M., Roberts S., Smith R., Linder S., O’Neil K., 2005, MNRAS, 357, 819  
 Sandage A., Bedke J., 1994, The Carnegie Atlas of Galaxies, (Washington DC: Carnegie Inst. of Washington with the Flintridge Foundation)  
 Sandage A., Tammann G. A., Yahil A., 1979, ApJ, 232, 352  
 Saracco P., D’Odorico S., Moorwood A., Buzzoni A., Cuby J.-G., Lidman C., 1999, A&A, 349, 751  
 Schechter P., 1976, ApJ, 203, 297  
 Schlegel D. J., Finkbeiner D. P., Davis M., 1998, ApJ, 500, 525  
 Schneider D. P., Gunn J. E., Hoessel J. G. 1983, ApJ, 264, 337  
 Secker J., Harris W. E., 1997, PASP, 109, 1364  
 Secker J., Harris W. E., Plummer J. D., 1997, PASP, 109, 1377  
 Sengupta C., Balasubramanyam R., 2006, MNRAS, 369, 360  
 Sérsic J. L., 1968, Atlas de galaxias australes. Córdoba, Argentina: Observatorio Astronómico  
 Servén J., Worthey G., 2010, AJ, 140, 152  
 Smith Castelli A. V., Bassino L. P., Richtler T., Cellone S. A., Aruta C., Infante L., 2008, MNRAS, 386, 2311  
 Smith Castelli A. V., Cellone S. A., Faifer F. R., Bassino L. P., Richtler T., Romero G. A., Calderón J. P., Caso J. P. 2011, MNRAS, in press (doi:10.1111/j.1365-2966.2011.19901.x)  
 Straizys V., Sviderskiene Z., 1972, VilOB, 35, 3  
 Tantalo R., Chiosi C., 2004, MNRAS, 353, 917  
 Thomas D., Maraston C., Bender R., 2003, MNRAS, 339, 897  
 Thuan T. X., & Gunn J. E. 1976, PASP, 88, 543  
 Tolstoy E., Hill V., Tosi M., 2009, ARA&Ap, 47, 371  
 Trager S. C., Worthey G., Faber S. M., Burstein D., Gonzalez J. J., 1998, ApJS, 116, 1  
 Trager S. C., Faber S. M., Worthey G., González J. J., 2000, AJ, 119, 1645  
 Wade R. A., Hoessel J. G., Elias J. H., Huchra J. P. 1979, PASP, 91, 35  
 Worthey G., Faber S. M., Gonzalez J. J., 1992, ApJ, 398, 69  
 Worthey G., Faber S. M., Gonzalez J. J., Burstein D., 1994, ApJS, 94, 687  
 Zandivarez A., Martinez H. J., 2011, MNRAS, 415, 2553  
 Zhu G., Blanton M. R., Moustakas J., 2010, ApJ, 722, 491

col. 1 - Galaxy ID (see, in this regard, Footnote 2);

col. 2 - Membership code,  $m_c$ : 1 = definite; 2 = likely; 3 = possible; 4 = non member. Membership is assigned according to: *i)*  $cz < 3800 \text{ km s}^{-1}$  if redshift is available from either CB05 and/or Mendel et al. (2008) and/or other, *ii)* morphology (if no redshift available).

col. 3 - Morphological classification according to CB05. See Cellone & Buzzoni (2007) for the meaning of “mixed” morphological classes;

col. 4 - Morphological classification according to FS90;

col. 5 - De Vaucouleurs’ morphological type,  $T$ ;

cols. 6 and 7 - Isophotal radius ( $\rho_{27}$ ) at  $\mu = 27 \text{ mag arcsec}^{-2}$ , and effective radius ( $\rho_e$ ), which encircles 50% of the luminosity within  $\rho_{27}$ . The  $g$ -band imagery is taken as a reference for the ESO sample, and  $V$ -band for the CASLEO galaxies;

cols. 8,9, and 10 - Sérsic fitting parameters from  $g$ -band (ESO sample) and  $V$ -band imagery (CASLEO sample). These are central brightness ( $\mu_0$ ) in  $\text{mag arcsec}^{-2}$ , scale radius ( $\rho_0$ ) in arcsec, and “shape index”  $n$ ;

col. 11 - Total apparent magnitude encircled within the  $\mu = 27 \text{ mag arcsec}^{-2}$  isophote in the  $g$  (ESO) and  $V$  (CASLEO) bands;

col. 12 - Mean surface brightness within  $\rho_{27}$  isophotal radius in the  $g$  (ESO) and  $V$  (CASLEO) bands;

col. 13 - Mean surface brightness within one effective radius  $\rho_e$  in the  $g$  (ESO) and  $V$  (CASLEO) bands;

col. 14 to 19 (Table A1) - Gunn *griz* colours within the  $g$ -band values of  $\rho_{27}$  and  $\rho_e$  for the ESO galaxies;

col. 14 to 15 (Table A2) - Johnson *BV* colours within the  $V$ -band values of  $\rho_{27}$  and  $\rho_e$  for the CASLEO galaxies.

## APPENDIX A: RELEVANT PROPERTIES OF THE NGC 5044 GROUP GALAXIES

We summarize in Tables A1 and A2 the main distinctive properties of the observed galaxy population in the NGC 5044 group. Column caption, for both tables is as follows:

Table A1. Morphological and photometric properties of the Eso galaxy sample

Name	Membership code	Classification		Morphological Type	$\rho_{27}''$ [arcsec]	$\rho_e''$	Sérsic fitting parameters			$g_{27}$ [mag]	$\mu_{g_{27}}$ [mag arcsec $^{-2}$ ]	$\langle\mu_{g_e}\rangle$ [mag arcsec $^{-2}$ ]	$(g-r)_{27}$	$(g-r)_e$	$(g-i)_{27}$	$(g-i)_e$	$(g-z)_{27}$	$(g-z)_e$
		CB05	FS90				$\mu_o$	$\rho_o$	$n$									
N17	1	S0pec	SdIV?	0	33.73	10.13	21.11±0.07	4.35±0.38	0.84±0.04	15.556	24.439	22.557	0.379	0.375	0.756	0.752	0.836	0.824
N20	1	dE-N	dE-N	-5	12.72	5.98	23.58±0.05	4.68±0.13	1.11±0.06	18.551	25.317	24.309	0.412	0.424	0.831	0.851	0.978	1.031
N24	1	Sm	Sm?	9	16.33	5.29	21.58±0.09	3.92±0.27	1.19±0.07	16.930	24.238	22.523	0.189	0.188	0.271	0.279	0.490	0.503
N30	1	dE	dE-N	-5	35.72	10.49	20.87±0.07	4.17±0.36	0.80±0.03	15.269	24.277	22.358	0.425	0.430	0.738	0.746	0.914	0.928
N31	1	Im	ImIV?	10	29.42	9.48	20.90±0.25	1.71±0.54	0.61±0.06	16.328	24.915	23.124	0.229	0.221	0.366	0.344	0.298	0.226
N32	1	S0	S0	0	58.00	10.70	16.90±0.33	0.97±0.33	0.55±0.04	13.171	23.232	20.305	0.459	0.454	0.763	0.747	1.008	1.008
N33	4	SB?c	bSp	5	12.07	4.13	21.90±0.03	3.47±0.08	1.21±0.03	17.569	24.221	22.610	0.210	0.211	0.314	0.315	0.413	0.438
N34	1	dE	d:E-N	-5	26.23	6.96	18.87±0.25	0.28±0.09	0.44±0.02	16.168	24.505	22.341	0.329	0.326	0.651	0.647	0.781	0.756
N39	4	E	E	-5	22.19	4.54	13.65±1.05	3E-4±0.00	0.22±0.02	16.507	24.481	21.728	0.541	0.531	0.859	0.844	1.092	1.078
N42	1	dE/dS0	dE-N	0	44.30	14.67	19.70±0.35	0.63±0.33	0.43±0.04	15.213	24.688	22.983	0.200	0.161	0.530	0.489	0.620	0.597
N49	1	ImIII	ImIII	10	25.60	7.92	21.57±0.03	6.96±0.18	1.30±0.04	15.751	24.036	22.222	0.052	0.047	0.207	0.209	0.387	0.402
N50	1	dE-Npec/BCD	dE-N	-5	26.20	7.50	20.39±0.07	4.52±0.31	1.03±0.04	15.218	23.556	21.591	0.409	0.407	0.650	0.645	0.808	0.801
N54	1	dI/dE	dE	10	43.55	18.02	22.94±0.04	11.10±0.30	1.00±0.05	15.825	25.263	24.016	0.192	0.160	0.451	0.427	-0.800	-0.103
N54A	2	dSph	dSph	-4	5.54	3.69	25.64±0.26	4.82±0.05	1.76±0.62	21.352	26.314	25.960	0.172	0.205	-0.206	-0.089	0.203	0.345
N55	1	dE/dI	dE	-5	9.37	5.67	23.45±0.16	2.11±0.32	0.82±0.10	19.664	25.767	25.140	0.369	0.367	0.414	0.426	0.597	0.632
N56	1	dSph	dE	-4	12.00	6.67	24.35±0.05	6.88±0.12	1.47±0.08	18.866	25.645	24.921	0.260	0.268	0.201	0.145	0.342	0.369
N62	1	dSph	dE	-4	9.76	5.65	24.79±0.06	6.43±0.25	1.26±0.08	19.657	25.849	25.360	0.355	0.354	0.479	0.482	0.436	-0.018
N64A	1	dSph	dSph	-4	9.85	5.35	24.61±0.05	6.10±0.11	1.92±0.11	19.534	25.746	25.119	0.286	0.267	0.478	0.452	0.059	0.430
N68	1	Sab(s)	Sab(s)	2	83.49	15.06	17.64±0.13	2.11±0.33	0.58±0.02	12.124	22.975	19.988	0.280	0.272	0.724	0.722	0.983	0.983
N70	1	dE-N/dI	dE	-5	23.00	10.70	23.36±0.04	7.92±0.17	1.14±0.05	17.227	25.278	24.241	0.352	0.339	0.692	0.687	0.906	0.904
N70A	2	dSph	dSph	-4	7.08	5.85	25.42±0.10	6.23±0.29	1.83±0.17	20.682	26.176	26.097	0.510	0.537	0.610	0.573	0.726	0.831
N71	1	dE-N?	dE-N	-5	27.50	7.62	18.70±0.51	0.16±0.12	0.40±0.05	16.427	24.868	22.749	0.379	0.360	0.598	0.559	0.773	0.730
N75	1	dE/dS0	d:E-N	0	29.96	7.19	19.73±0.18	1.73±0.36	0.66±0.04	15.326	23.952	21.592	0.378	0.379	0.678	0.677	0.861	0.863
N83	1	dE	dE	-5	29.63	12.36	22.75±0.06	6.38±0.35	0.91±0.05	16.667	25.269	24.018	0.393	0.416	0.722	0.730	0.890	0.871
N83A	2	dSph	dSph	-4	9.68	6.08	24.86±0.08	4.81±0.11	1.07±0.09	20.057	26.230	25.779	0.229	0.288	0.286	0.293	0.400	0.383
N89	1	dE-N	dE-N	-5	21.64	8.22	21.92±0.12	2.32±0.33	0.71±0.05	17.258	25.177	23.752	0.318	0.304	0.625	0.616	0.806	0.804
N90	4	Sc	dE-N	5	8.23	3.38	22.66±0.09	2.27±0.16	0.99±0.06	18.928	24.748	23.550	0.042	0.057	0.274	0.295	0.425	0.458
N93	3	Sm(bg?)	bSp	9	12.75	4.25	21.53±0.09	2.68±0.21	1.08±0.06	17.538	24.310	22.646	0.067	0.059	0.255	0.251	0.388	0.419
N93A	1	dSph	dSph	-4	14.53	8.83	25.14±0.04	10.60±0.30	2.15±0.07	18.960	26.015	25.503	0.295	0.276	0.589	0.564	0.762	0.767
N93B	2	dSph	dSph	-4	5.85	3.38	25.01±0.12	2.93±0.02	1.83±0.22	21.461	26.540	25.971	0.235	0.209	0.624	0.543	0.810	0.974
N93C	2	dE-N	dE-N	-5	8.31	5.85	24.40±0.07	4.36±0.06	1.50±0.12	19.895	25.738	25.346	0.275	0.146	0.515	0.478	0.422	0.433
N109	4	Sdm	ImV	8	16.71	7.34	22.57±0.04	4.09±0.18	0.96±0.04	17.583	24.942	23.852	0.185	0.176	0.209	0.168	0.348	0.298
N134	1	Sm	Sm	9	37.77	7.37	19.20±0.04	1.43±0.09	0.64±0.01	15.021	24.149	21.332	-0.093	-0.112	-0.079	-0.095	0.012	0.042
N138	1	dE-N	dE-N	-5	15.50	6.58	22.38±0.15	2.49±0.38	0.81±0.08	18.027	25.230	23.994	0.279	0.278	0.446	0.437	0.526	0.519
N139	3	E(bg?)	E	-5	16.18	3.77	16.20±1.18	0.01±0.03	0.34±0.06	17.227	24.515	22.062	1.217	1.196	1.471	1.432	1.732	1.701
N152	4	Sd	SmIII	7	18.17	6.22	22.10±0.03	6.46±0.10	1.61±0.05	16.611	24.151	22.554	0.130	0.141	0.302	0.312	0.550	0.572
N153	1	d:S0	d:S0	0	47.16	11.63	19.39±0.19	1.20±0.29	0.53±0.03	14.772	24.383	22.060	0.392	0.384	0.729	0.721	0.917	0.916
N155	1	Sab	Sm	2	23.35	6.43	20.51±0.11	2.28±0.26	0.78±0.04	16.181	24.265	22.193	0.375	0.374	0.572	0.564	0.711	0.704
N156	1	dI/dE	dE	10	30.98	14.75	23.52±0.04	9.15±0.16	1.04±0.05	16.916	25.614	24.621	0.249	0.204	0.395	0.329	0.438	0.393
B3	4	E	E	-5	10.15	2.40	19.29±0.08	0.45±0.05	0.62±0.02	17.637	23.914	21.514	0.576	0.575	0.905	0.894	1.140	1.142

Table A2. Morphological and photometric properties of the CASLEO galaxy sample

Name	Membership code	Classification CB05	FS90	Morphological Type	$\rho_{27}''$ [arcsec]	$\rho_e''$	Sérsic fitting parameters			$V_{27}$ [mag]	$\mu V_{27}$ [mag arcsec $^{-2}$ ]	$\langle\mu V_e\rangle$	(B-V) $_{27}$	(B-V) $_e$
							$\mu_o$	$\rho_o$	$n$					
N18	1	E?/Sab	Sab	1	75.14	14.78	17.80±0.24	0.93±0.27	0.48±0.03	13.072	23.694	20.904	...	...
N19	1	Sm	dE	9	17.50	6.06	21.55±0.06	3.04±0.17	0.91±0.03	17.027	24.485	22.920	...	...
N29	1	d:E	d:E	-5	41.41	9.63	18.76±0.22	0.79±0.20	0.51±0.03	14.809	24.138	21.686	0.875	0.876
N30	1	dE	dE-N	-5	38.43	10.97	20.39±0.12	2.99±0.37	0.70±0.03	15.105	24.271	22.255	0.866	0.868
N34	1	dE	d:E-N	-5	26.34	6.95	19.84±0.27	1.13±0.32	0.60±0.05	15.984	24.331	22.151	0.854	0.842
N38	1	d:E	E	-5	17.00	4.08	18.32±0.42	0.27±0.11	0.50±0.04	16.676	24.071	21.677	0.910	0.908
N42	1	dE/dS0	dE-N	0	43.31	13.45	20.89±0.13	3.83±0.55	0.70±0.04	15.031	24.457	22.619	0.813	0.794
N46	4	Scd	dE,N	6	13.98	5.40	21.95±0.05	3.41±0.14	1.07±0.03	17.504	24.475	23.129	0.629	0.631
N46A	2	dSph		-4	7.78	4.45	24.76±0.02	5.30±0.02	1.92±0.04	20.075	25.773	25.159	0.774	0.817
N49	1	ImIII	ImIII	10	23.82	8.30	21.52±0.04	7.20±0.21	1.35±0.04	15.736	23.863	22.304	0.397	0.399
N49A	2	dSph		-4	6.78	5.00	24.49±0.06	2.88±0.08	0.96±0.06	20.631	26.030	25.724	0.882	0.792
N50	1	dE-Npec/BCD	dE-N	-5	25.93	7.26	20.14±0.07	4.22±0.26	1.01±0.03	15.058	23.369	21.334	0.805	0.805
N51	1	dE/dS0	dE,N	0	39.89	14.03	20.47±0.26	1.08±0.38	0.50±0.04	15.715	24.962	23.326	0.893	0.942
N52	4	S	dE,N	4	7.65	3.19	23.55±0.03	3.97±0.04	1.83±0.06	19.239	24.899	23.693	0.670	0.634
N53	1	d:E	BCD?	-5	18.05	3.65	17.35±0.85	0.20±0.13	0.48±0.06	15.983	23.509	20.770	1.045	1.054
N54	1	dI/dE	dE	10	39.50	16.09	22.83±0.04	10.70±0.35	1.05±0.04	15.883	25.108	23.845	0.804	0.784
N54A	2	dSph		-4	5.60	4.80	24.90±0.11	3.21±0.18	1.21±0.10	21.099	26.081	25.954	0.953	0.921
N55	1	dE/dI	dE	-5	10.14	5.50	23.37±0.24	2.18±0.54	0.80±0.11	19.446	25.718	24.907	0.553	0.393
N56	1	dSph	dE	-4	15.70	8.22	23.96±0.04	5.93±0.11	1.02±0.04	18.458	25.681	24.904	0.896	0.863
N57	1	dE,N	dE	-5	16.68	9.03	23.85±0.10	6.42±0.43	1.12±0.08	18.206	25.559	24.750	0.903	0.995
N58	1	Im/dE	dE/Im	10	15.77	6.09	21.55±0.17	1.16±0.24	0.63±0.05	17.986	25.219	23.821	0.827	0.716
N61	2	dSph	dE/Im	-4	8.12	4.36	23.91±0.09	3.08±0.18	1.07±0.07	19.851	25.643	24.897	0.834	0.821
N62	1	dSph	dE	-4	18.22	12.15	24.21±0.04	6.79±0.16	0.91±0.04	18.354	25.900	25.389	1.266	1.422
N63	1	S0	dS0	0	66.19	19.05	20.35±0.10	4.35±0.47	0.66±0.03	13.992	24.339	22.350	0.886	0.871
N66	1	dE	dE,N	-5	25.62	9.12	21.56±0.09	3.06±0.27	0.76±0.03	16.537	24.822	23.248	0.794	0.801
N70	1	dE-N/dI	dE	-5	23.37	10.62	23.13±0.08	7.52±0.45	1.12±0.07	17.082	25.167	24.099	0.976	0.959
N70A	2	dSph		-4	9.59	7.19	25.45±0.05	7.82±0.16	1.62±0.08	20.011	26.163	25.935	0.756	0.778
N72A	2	dSph		-4	7.99	5.60	24.68±0.05	4.59±0.03	1.32±0.06	20.134	25.891	25.501	0.854	0.973
N73	3	dSph(bg?)	dE	-4	6.74	3.84	24.15±0.03	3.27±0.01	1.29±0.05	20.209	25.595	24.943	0.753	0.731
N75	1	dE/dS0	d:E-N	0	30.76	7.38	19.79±0.11	2.15±0.25	0.71±0.03	15.210	23.893	21.529	0.892	0.891
N76	1	dE	d:E	-5	23.58	4.73	17.39±0.34	0.21±0.08	0.46±0.03	15.653	23.758	21.004	0.923	0.910
N79	1	dE/dS0	E	0	25.19	5.85	19.67±0.15	1.69±0.26	0.70±0.04	15.536	23.785	21.347	0.860	0.837
N80	2	dE(bg?)	dE	-5	9.57	4.98	23.87±0.21	4.40±0.49	1.38±0.15	19.252	25.399	24.590	1.106	1.147
N80A	3	Im/dE(bg?)		10	9.59	6.39	24.11±0.13	3.27±0.39	0.96±0.11	19.835	25.988	25.444	0.712	0.897
N82	1	S0/a	S0/a	0	42.53	11.62	20.33±0.05	7.37±0.32	1.02±0.03	14.033	23.419	21.339	0.893	0.890
N82A	2	dSph		-4	6.39	4.80	25.34±0.06	4.70±0.03	1.30±0.09	20.987	26.258	26.001	0.884	0.805
N83	1	dE	dE	-5	27.91	11.28	22.66±0.03	7.40±0.19	1.05±0.03	16.509	24.981	23.700	1.036	1.024
N83A	2	dSph		-4	9.98	6.54	24.96±0.04	6.38±0.07	1.29±0.05	19.781	26.012	25.605	0.809	0.751
N85	3	E(bg?)	dE	-5	13.97	5.73	21.73±0.43	1.24±0.53	0.66±0.08	18.251	25.219	23.887	1.149	1.157
N94	1	d:E/S0	d:E	0	39.97	9.30	19.43±0.23	1.46±0.37	0.58±0.04	14.800	24.052	21.607	0.920	0.918
N94A	2	dSph		-4	7.99	5.20	25.03±0.10	4.45±0.23	0.95±0.09	20.461	26.217	25.855	0.834	0.827
N94B	2	dSph		-4	9.19	5.60	24.51±0.04	3.29±0.06	0.81±0.03	20.081	26.141	25.592	0.792	0.781
N95	1	dE	dE,N?	-5	16.43	6.53	21.76±0.03	2.16±0.08	0.77±0.02	17.571	24.891	23.500	0.842	0.755
N95A	1	dSph		-4	16.19	10.41	23.43±0.06	2.62±0.20	0.66±0.03	18.591	25.880	25.324	0.936	0.895
N98	3	Im/dE(bg?)	dE	10	10.16	4.35	22.59±0.07	1.86±0.12	0.86±0.03	19.068	25.344	24.140	1.067	1.084
N108	1	dE	dE,N	-5	15.59	4.64	20.87±0.08	2.28±0.16	0.90±0.03	16.900	24.106	22.207	0.883	0.887
N109	4	Sdm	ImV	8	15.87	7.00	23.06±0.05	6.51±0.16	1.34±0.04	17.524	24.770	23.706	0.645	0.626
N116	1	d:E	dE,N	-5	10.09	4.35	22.09±0.11	1.34±0.15	0.73±0.04	18.813	25.075	23.876	0.751	0.760
N117	1	dE/dS0	d:E,N	0	28.66	7.35	20.10±0.07	4.31±0.25	0.97±0.03	14.857	23.386	21.172	0.911	0.909
N122	1	dE	dE	-5	22.05	8.35	21.62±0.12	2.35±0.30	0.71±0.04	16.965	24.925	23.504	0.752	0.732
N124	4	E(bg)	dE	-5	17.57	6.78	20.25±0.21	0.29±0.08	0.45±0.02	17.760	25.226	23.768	0.928	0.938
N131	1	S0	d:S0	0	35.67	8.82	19.75±0.11	2.36±0.28	0.69±0.03	14.812	23.817	21.516	...	...
N131A	2	dSph		-4	11.19	6.39	23.03±0.08	1.45±0.15	0.64±0.04	19.298	25.785	25.015	...	...
N136	4	S(bg)	BCD?	4	8.54	2.67	20.50±0.06	1.90±0.07	1.18±0.03	17.517	23.418	21.640	...	...
N149	1	Im/dE	dE	10	20.06	7.76	22.50±0.11	5.37±0.44	1.08±0.07	17.068	24.822	23.468	0.850	0.830
N153	1	d:S0	d:S0	0	48.83	11.95	19.29±0.14	1.33±0.23	0.55±0.02	14.606	24.292	21.953	0.855	0.854
B3	4	E		-5	10.87	2.43	17.91±0.38	0.17±0.06	0.51±0.04	17.406	23.831	21.288	1.445	1.451



**Table A3.** Coordinates of the 6 new dSph galaxies discovered in the CASLEO fields

Name	$\alpha_{J2000}$	$\delta_{J2000}$
N46A	13 <sup>h</sup> 14 <sup>m</sup> 19.1 <sup>s</sup>	−16° 17′ 32″
N72A	13 <sup>h</sup> 14 <sup>m</sup> 51.8 <sup>s</sup>	−15° 56′ 28″
N80A	13 <sup>h</sup> 15 <sup>m</sup> 11.8 <sup>s</sup>	−16° 59′ 48″
N82A	13 <sup>h</sup> 15 <sup>m</sup> 23.4 <sup>s</sup>	−16° 27′ 18″
N94A	13 <sup>h</sup> 15 <sup>m</sup> 34.2 <sup>s</sup>	−16° 30′ 36″
N94B	13 <sup>h</sup> 15 <sup>m</sup> 39.7 <sup>s</sup>	−16° 29′ 56″

**Table A4.** Coordinates of background “bonus” galaxies.

Name	$\alpha_{J2000}$	$\delta_{J2000}$
B1	13 <sup>h</sup> 14 <sup>m</sup> 19.0 <sup>s</sup>	−16° 10′ 38″
B2	13 <sup>h</sup> 15 <sup>m</sup> 02.1 <sup>s</sup>	−16° 22′ 17″
B3	13 <sup>h</sup> 16 <sup>m</sup> 07.4 <sup>s</sup>	−17° 00′ 08″
B4	13 <sup>h</sup> 17 <sup>m</sup> 41.9 <sup>s</sup>	−16° 10′ 07″
B5	13 <sup>h</sup> 14 <sup>m</sup> 00.0 <sup>s</sup>	−15° 56′ 35″
B6	13 <sup>h</sup> 17 <sup>m</sup> 42.7 <sup>s</sup>	−16° 32′ 48″

This paper has been typeset from a  $\text{\TeX}$ / $\text{\LaTeX}$  file prepared by the author.